

000 MUONBP: FASTER MUON VIA BLOCK-PERIODIC OR- 001 002 THOGONALIZATION 003 004

005 **Anonymous authors**

006 Paper under double-blind review

007 008 ABSTRACT 009

011 Gradient orthogonalization is a simple strategy that shows great utility in speed-
012 ing up gradient descent. The Muon optimizer (Jordan et al., 2024b) combines
013 gradient orthogonalization with first-order momentum and achieves significant
014 improvement in data efficiency over Adam/AdamW for language model training.
015 However, when using model parallelism, gradient orthogonalization introduces
016 additional overhead compared to coordinate-wise optimizers (such as AdamW)
017 due to additional gather and scatter operations on gradient matrix shards from
018 different devices. This additional communication can amount to a throughput
019 hit of 5%-10% compared to Adam/AdamW. To remedy this, we propose Muon
020 with Block-Periodic Orthogonalization (MuonBP), which applies orthogonaliza-
021 tion independently to matrix shards on each device and periodically performs full
022 orthogonalization to maintain training stability at scale. We show how to ad-
023 just the learning rate from the baseline to MuonBP and give convergence guar-
024 antees for this algorithm. Crucially, our theory dictates that we use two stepsizes:
025 one for the blockwise orthogonalization steps, and one for the full orthogonaliza-
026 tion steps. Our method is simple, requires minimal hyperparameter adjustments,
027 and achieves competitive iteration complexity compared with the baselines Muon
028 and Dion while providing per-iteration throughput comparable to coordinate-wise
029 methods such as AdamW. When training an 8B model with eight-way tensor par-
030 allelism and ZeRO optimizer state sharding, MuonBP achieves 8% throughput
031 increase compared to Muon with no degradation in performance.

032 1 INTRODUCTION

033
034 First order optimization methods have been the staple in the success of deep learning in the last
035 decade. In particular, Adam (Kingma & Ba, 2015; Loshchilov & Hutter, 2019a) has become the
036 *de facto* standard across both industry and academia. Despite numerous attempts to improve upon
037 Adam’s performance, it has remained unchallenged as the optimizer of choice for training large-
038 scale neural networks. But this wall might be starting to crack. A recent newcomer, Muon (Jor-
039 dan et al., 2024b), consistently outperforms Adam on various LLM training tasks ranging from
040 small scale benchmarks to larger LLM training setting with up to 1T model parameters Team et al.
041 (2025). Muon is more data efficient than Adam, requiring fewer tokens to reach the same valida-
042 tion loss (Liu et al., 2025). It also enjoys a higher critical batch size, which allows for further use
043 of parallelism (Essential AI et al., 2025) to accelerate training. Both of these aspects are critical
044 in large-scale LLM pretraining, where even marginal efficiency gains can translate into substantial
045 computational and financial savings.

046 Muon orthogonalizes the update matrix for each layer before using it in a descent step, and it
047 can be seen as a form of steepest descent (Bernstein, 2025) or as a Non-Euclidean Trust Region
048 method (Kovalev, 2025). A key disadvantage of Muon, compared to Adam, is that orthogonaliza-
049 tion is not a coordinate-wise operation. Rather, it requires gathering the gradient matrix from
050 different devices whenever model parallelism is used. This introduces additional throughput over-
051 head compared to Adam (Essential AI, 2025). Although Muon is more *token efficient*, it is strictly
052 slower than Adam on a per-iteration basis under model parallelism.

053 The goal of this work is to bridge this throughput gap while preserving the data efficiency of Muon.
054 To this end, we propose Muon with Block-Periodic orthogonalization (MuonBP, Algorithm 1).

MuonBP block-orthogonalizes the matrix shards on each device independently and periodically gathers the shards for a full orthogonalization. In the off-period iterations, MuonBP does not require any additional communication, recovering the communication efficiency of Adam. However, orthogonalizing shards only is not enough for a competitive performance. We observe this block-only variant (BlockMuon, (Boreiko et al., 2025)) suffers from a potentially worse convergence guarantee and fails as the models scale up. Hence, we introduce periodic global orthogonalization steps. Combined, MuonBP recovers the performance of Muon with a drastic reduction in communication overhead. Our main contributions are as follows.

- We propose MuonBP, a variant of Muon with local orthogonalization interleaved with periodic full orthogonalization. In the off-period iterations, MuonBP treats each tensor parallel shard independently and orthogonalizes it separately. In the on-period iterations we gather the tensors and do a full orthogonalization. Our experiments with a period of 5 indicate that we recover the performance of Muon with $5\times$ reduction in the optimizer step communication volume.
- We provide a theoretical analysis of the algorithm (Theorem 2) that shows (a) the blocking period P smoothly interpolates between the convergence rate of Muon and BlockMuon, that (b) we should use *two different learning rates* in the blocking vs full iterations, and finally (c) gives us guidance on how to scale the learning rate when using block orthogonalization.
- Empirically, we show that MuonBP converges faster than the baseline (non-blocking) Muon algorithm (Jordan et al., 2024b), Dion (Ahn et al., 2025), AdamW (Kingma & Ba, 2015; Loshchilov & Hutter, 2019b), and BlockMuon (Boreiko et al., 2025) in practical pretraining tasks in terms of the wall-clock time. We observe that our method recovers the original Muon’s performance with a up to 8% increase in throughput under layerwise sharding and tensor parallelism.

We briefly outline the rest of this paper. In Section 2, we provide necessary background for a steepest descent view of Muon, which will be useful for other sections. We discuss related work and compare our work to few others who examined orthogonalized updates in large scale distributed settings. In Section 3, we discuss our algorithm with convergence analysis, our goal is to analyze the effect of periodicity in the behaviour of our algorithm. Finally, in Section 4, we examine our algorithm in billion-scale training settings and compare to other baselines in terms of accuracy and throughput.

2 BACKGROUND AND RELATED WORK

Optimizers as steepest descent. Bernstein & Newhouse (2024b) argued for viewing different optimizers as steepest descent under different norms. This perspective is very useful in analyzing Muon as it (a) clarifies what Muon is optimizing *for*, and (b) gives a common template to compare Muon, its blockwise variants, and coordinate-wise methods like Adam. For example, when EMA is turned off in Adam, it reduces to sign descent. We may observe that for any $x \in \mathbb{R}^d$ and a differentiable function f

$$\arg \min_{\Delta x \in \mathbb{R}^d} \left(f(x) + \langle \nabla f(x), x + \Delta x \rangle + \frac{\lambda}{2} \|\Delta x\|_\infty^2 \right) = -\frac{\|\nabla f(x)\|_1}{\lambda} \text{sign}(\nabla f(x)), \quad (1)$$

where $\|u\|_\infty = \max_{i=1,\dots,d} |u_i|$. The steepest descent view results in the additional scaling by $\|\nabla f(x)\|_1$ in the numerator. This scaling factor results in different parameter update norm every iteration ($\propto \|\nabla f(x)\|_1$). We can instead explicitly control the parameter update norm by using the Non-Euclidean Trust Region (NTR) formulation. This is the formulation used by Kovalev (2025): at iterate x , NTR minimizes the first-order model of f over a norm ball $\{\Delta : \|\Delta\| \leq 1/\lambda\}$, which yields the steepest-descent direction in that norm. For $\|\cdot\|_\infty$ this recovers (unscaled) sign descent. The NTR formulation also allows for elegant theoretical analysis, including incorporating algorithmic techniques such as momentum (Kovalev, 2025). For these reasons, we will adopt the NTR framework as our algorithmic template in Section 3.

Muon. Changing the norm used from $\|\cdot\|_\infty$ to any other norm opens up a large design space of optimization algorithms. For example, we may use different norms for different parameters in a neural network. If the parameter X of a certain layer is a matrix of dimensions $m \times n$, using the operator norm $\|X\|_{\text{op}} = \sup_{z \in \mathbb{R}^n} \frac{\|Xz\|}{\|z\|}$ instead gives

$$\arg \min_{\Delta X \mid \|\Delta X\|_{\text{op}} \leq \frac{1}{\lambda}} (f(X) + \langle \nabla f(X), X + \Delta X \rangle) = -\frac{1}{\lambda} \text{Orth}(\nabla f(X)), \quad (2)$$

108 where $\text{Orth}(U) = (UU^\top)^{-\frac{1}{2}}U$. If we use Newton-Schulz iterations (Algorithm 2) to approxi-
 109 mately compute the orthogonalization and apply the maximization to a running momentum buffer in-
 110 stead of the gradient directly, we obtain Muon (Jordan et al., 2024b). Bernstein & Newhouse (2024a)
 111 argue for using layer-dependent norms depending on the expected norm for the input vs output of
 112 each layer. In practice, the choice of norm is also motivated by empirical performance (Jordan et al.,
 113 2024b). If we instead use the $\ell_1 \rightarrow \ell_2$ -induced norm, we obtain column normalization. That is, given
 114 a stochastic gradient $G = [G_{:,1} \quad G_{:,2} \quad \cdots \quad G_{:,n}]$, we set $\Delta X = -\frac{1}{\lambda} \begin{bmatrix} \frac{G_{:,1}}{\|G_{:,1}\|} & \cdots & \frac{G_{:,n}}{\|G_{:,n}\|} \end{bmatrix}$.
 115 This was used for the first layer in Scion (Pethick et al., 2025) and for every layer save the last in
 116 SCALE (Glentis et al., 2025). Glentis et al. (2025) show that this using column normalization with
 117 momentum on the last layer allows for training transformers competitive with Adam and Muon for
 118 up to 1B parameters scale.

119 The choice of norm dictates the operation to be done at every step and its structure (e.g. coordinate-
 120 wise vs. matrix-wise). This, in turn, determines both the computational cost of the update and
 121 whether distributed execution requires cross-device collectives.

122 **Computational costs.** For a parameter matrix of size $m \times n$, the per-step cost of SGD with Mo-
 123 mentum is just $2mn$ floating point operations and $4mn$ FLOPs for Adam. In comparison, orthogonaliza-
 124 tion is more expensive. Using K Newton-Schulz iterations (Algorithm 2 in the Appendix), the total
 125 is $2mn + 2K(2nm^2 + m^3)$ FLOPs assuming without loss of generality that $m \leq n$ (Jordan et al.,
 126 2024b). Some approaches to reducing the computational cost of orthogonalization include tuning
 127 a, b, c in Algorithm 2 to reduce the number of steps needed (Jordan et al., 2024b) or using adaptive
 128 per-step a, b, c (Amsel et al., 2025). Note that this computational cost might be small relative to the
 129 forward and backward passes in backpropagation. A common rule of thumb is fwd+bwd computa-
 130 tion $\approx 6NT$ FLOPs for a dense network with N params and input size of T tokens. For larger batch
 131 sizes, this becomes more dominant as the optimizer step is independent of the input size.

132 **Communication costs.** Modern neural networks are trained with a combination of data and model
 133 parallelism. Data Parallelism (DP) replicates model parameters, gradients, and optimizer states
 134 across the communication network but passes different data batches to each DP group. The gradi-
 135 ents are synchronized across the different devices before applying the optimizer step. While this
 136 replicates the optimizer step computation across different DP groups, it adds no additional com-
 137 munication cost. In contrast, model parallelism typically will shard some or all of these tensors.
 138 Tensor Parallelism (Shoeybi et al., 2019) (TP) shards the model parameters for both storage and
 139 computation; This sharding is done along one or more dimensions (e.g. row, column) of each ten-
 140 sor. Pipeline Parallelism (Huang et al., 2018) (PP) also shards model parameters for both storage
 141 and computation, but does so by dividing the layers among different PP groups. The Zero Redun-
 142 dancy Optimizer (Rajbhandari et al., 2019) (ZeRO), Fully Sharded Data Parallelism (Zhao et al.,
 143 2023) (FSDP), and FSDP2 (Liang et al., 2024) shard model parameters either by layer or on the
 144 first dimension, but do that for the purpose of saving memory. Before doing the forward/backward
 145 computation involving a certain layer, ZeRO/FSDP2 undo the sharding they apply first.

146 **Communication cost of Muon.** There are several strategies for parallelizing Muon and they deter-
 147 mine the communication costs involved (Essential AI, 2025). If we use TP or FSDP2, we have to
 148 do an additional all-gather across the TP/FSDP2 groups to gather the model parameters. A naive
 149 all-gather would force us to orthogonalize the same matrix in parallel which is redundant. A better
 150 alternative is to use two all-to-all communications to redistribute different layer tensors. This suffers
 151 from two issues: (a) we still have to do two additional collective operations, and (b) if the number of
 152 matrices to be orthogonalized is larger than the number of GPUs, some GPUs would sit idle. If we
 153 use ZeRO, then the fact that the optimizer states, parameters, and gradients are already sharded layer-
 154 wise helps greatly: we do not need to do an all-gather across the distributed optimizer groups and
 155 can apply orthogonalization layerwise in parallel. In this case, the only extra communication cost
 156 we suffer from comes from all-gathering across the TP groups. For an 8B parameter LLaMa-style
 157 transformer, this gives a throughput reduction of 8%-10%

158 This additional communication burden has motivated the development of Dion (Ahn et al., 2025)
 159 and, concurrently to our work, Boreiko et al. (2025) introduce a variant of BlockMuon (Algorithm 1
 160 with $P = \infty$). Dion (Ahn et al., 2025) maintains a low-rank approximation of the momentum matrix
 161 and distributes the orthogonalization process. For large enough batch sizes, Dion’s computational

162 cost is perfectly divided by the number of devices and its communication cost scales with the smaller
 163 rank.

164 **Other preconditioning algorithms.** Many of the same computational and communication
 165 constraints discussed above also apply to other gradient preconditioning algorithms, e.g. Sham-
 166 poo (Gupta et al., 2018), K-FAC (Martens & Grosse, 2015), and ASGO/One-Sided Shampoo (An
 167 et al., 2025; Xie et al., 2025). Distributed Shampoo (Shi et al., 2023) uses blocking, intermittent
 168 preconditioner updates, and layer-wise sharding similar to ZeRO-1/FSDP to reduce the amount of
 169 communication.

171 3 ALGORITHMS AND CONVERGENCE

173 Our starting point is the observation that column- or row-wise normalization can be viewed as or-
 174 thogonalization applied on a submatrix of size $m \times 1$ or $1 \times n$. An intermediate method between
 175 row-wise normalization and column-wise normalization would be orthogonalizing submatrices of
 176 dimensions $p \times q$ each where $p \leq m$ and $q \leq n$. This has two benefits,

- 177 • We reduce the amount of floating point operations per Newton-Schulz step from $2(2nm^2 + m^3)$
 178 to $2(2pq^2 + q^3) \times \frac{mn}{pq} = 2(2mnq + \frac{mnq^2}{p})$ floating point operations (assuming without loss of
 179 generality that $p \leq q$). For example, the MLP layers in LLaMA 3 405B (Grattafiori et al., 2024)
 180 have $m, n \in \{53248, 16384\}$. Here, orthogonalizing submatrices with 8-way TP gives a speedup
 181 of $\approx 2.36 \times$ for the up-projection and $\approx 9.06 \times$ for the down-projection per Newton–Schulz step
 182 relative to full orthogonalization.
- 183 • If we use *blocks* corresponding to the model parallelism used, we can entirely eliminate orthogo-
 184 nalization’s communication overhead under *any* regime. We discuss this in more detail below.

186 **How blocks align with model-parallel shards.** We divide each parameter, gradient, and opti-
 187 mizer state tensor into blocks and define each of these blocks to be exactly the tensor shard that
 188 resides on a device under the chosen model-parallelism layout. This makes the communication
 189 pattern explicit and ensures that a “block” step never requires cross-device traffic.

190 • *Tensor Parallelism (TP).* In Megatron-style (Shoeybi et al., 2019) *column-parallel* linear layers, a
 191 weight $W \in \mathbb{R}^{m \times n}$ is split by columns across c TP ranks, so each rank holds $W^{(j)} \in \mathbb{R}^{m \times (n/c)}$
 192 and produces a local gradient shard $G^{(j)} \in \mathbb{R}^{m \times (n/c)}$. A *block* is $G^{(j)}$; block-orthogonalization
 193 acts on $m \times (n/c)$ matrices and needs no gather/scatter. In *row-parallel* layers, W is split by
 194 rows across r ranks, so each shard is $((m/r) \times n)$ and the block is $G^{(i)} \in \mathbb{R}^{(m/r) \times n}$. For hybrid
 195 2D TP (row \times column), the global W is partitioned into an $r \times c$ grid of rectangular shards
 196 $((m/r) \times (n/c))$. TP is often applied not just to the linear layer but also to the attention weights
 197 as well, and the same discussion applies.

198 • *FSDP2 (dim-0 sharding).* When parameters are sharded only for memory (layer/dim-0), each
 199 rank holds a contiguous slice along the first dimension. During the optimizer step, *block* denotes
 200 this local slice; thus block-orthogonalization again requires no parameter all-gather. The same
 201 definition applies under TP+FSDP: the block is the intersection of the TP and FSDP partitions,
 202 i.e., a single $(\frac{m}{r_{\text{row}}} \times \frac{n}{c_{\text{col}}})$ shard.

203 In order to develop algorithms that minimize communication, we want to do block-wise operations
 204 as much as possible and keep “global” operations to a minimum. To this end, we analyze the variant
 205 of Muon that only does blockwise operations in Section 3.1. Our analysis shows that in the worst
 206 case, the convergence of this variant might be much worse than full Muon. To remedy this, we
 207 develop and analyze our block-periodic variant in Section 3.2.

210 3.1 BLOCK ORTHOGONALIZATION

212 BlockMuon (Algorithm 1 with $P = \infty$) applies orthogonalization to these blocks, in parallel, on
 213 different devices (Boreiko et al., 2025). This removes the need for any added communication and
 214 reduces the computational cost of orthogonalization. To better understand the convergence of Block-
 215 Muon, we analyze the algorithm under the assumptions of smoothness, bounded stochastic gradient
 variance, and norm equivalence characterized by ρ . We state our assumptions more clearly below.

216 **Assumption 1** (Smoothness). *We assume that $f : \mathbb{R}^{m \times n} \rightarrow \mathbb{R}$ is L -smooth with respect to a norm*
 217 *$\|\cdot\|$. That is, let $\|\cdot\|_*$ be the corresponding dual norm, then for all $X, Y \in \mathbb{R}^{m \times n} \rightarrow \mathbb{R}$ we assume*
 218 *$\|\nabla f(X) - \nabla f(Y)\|_* \leq L\|X - Y\|$.*

219 **Assumption 2** (Bounded Variance). *Suppose that the stochastic gradients $G(X)$ are (a) unbiased,*
 220 *$\mathbb{E}_\xi [G(X; \xi)] = \nabla f(X)$, and (b) have bounded variance $\mathbb{E}_\xi [\|G(X; \xi) - \nabla f(X)\|^2] \leq \sigma^2$.*

222 **Assumption 3** (Norm Equivalence). *The norm $\|\cdot\|$ satisfies $\|X\| \leq \rho\|X\|_F$ for some $\rho > 0$.*

224 As mentioned before, we will use the Non-Euclidean Trust Region (NTR) template (provided next)
 225 to analyze both algorithms.

$$226 \quad M_t = \mu M_{t-1} + G_t, \quad X_{t+1} = \arg \min_{X: \|X - X_t\| \leq \eta} \langle M_t, X - X_t \rangle, \quad (\text{NTR})$$

229 where G_t is a stochastic gradient with expectation $\nabla f(X_t)$. This framework was adopted for the
 230 convergence analysis of Muon by Kovalev (2025) and the next theorem is a slight modification of
 231 Theorem 2 in their work. The proof is also similar to (Li & Hong, 2025, Theorem 2.1).

232 **Theorem 1.** *Suppose that the function f satisfies Assumptions 1 to 3 and that f is lower bounded*
 233 *by f_* . Then for any $\eta > 0$ and $\mu \in [0, 1]$ the iterates generated by equation NTR satisfy*

$$234 \quad \mathbb{E} [\min_{t=0, \dots, T-1} \|\nabla f(X_t)\|_*] \leq \frac{f(X_0) - f_*}{\eta T} + \frac{3\sqrt{L(f(X_0) - f_*)}}{T} \frac{\mu}{1 - \mu} \\ 235 \quad + \frac{2(1 - \mu)\rho\sigma}{T} + \frac{L\eta\mu}{1 - \mu} + \rho\sigma\sqrt{\frac{1 - \mu}{1 + \mu}} + \frac{L\eta}{2}. \quad (3)$$

240 Theorem 1 applies to Muon, since under $\|\cdot\| = \|\cdot\|_{\text{op}}$, eq. (NTR) reduces to orthogonalizing
 241 momentum. The next lemma shows that Block-Muon can also be studied in the same framework.

242 **Lemma 1** (Dual of the Block-Spectral Norm). *Let $X \in \mathbb{R}^{m \times n}$ be partitioned into $r \times c$ blocks.*
 243 *Define the **block-spectral norm** as $B(X) = \max_{1 \leq i \leq r, 1 \leq j \leq c} \|X_{i,j}\|_{\text{op}}$. Its dual norm is $B^*(X) =$*
 244 *$\sum_{i,j} \|X_{i,j}\|_{\text{op},*}$, where $\|\cdot\|_*$ is the nuclear norm.*

245 BlockMuon is just eq. (NTR) with $\|\cdot\| = B(\cdot)$. To compare between the convergence of Muon and
 246 BlockMuon, we consider the simplified setting when $\sigma = 0$ and apply Theorem 1. Minimizing
 247 Equation (3) over η and μ yields $\eta_{\text{op},*} = \sqrt{\frac{2(f(X_0) - f_*)}{TL_{\text{op}}}}$ and $\mu = 0$ and the convergence guarantee
 248 $\|\nabla f(X_\tau)\|_{\text{op},*} \leq \sqrt{\frac{2L_{\text{op}}(f(X_0) - f_*)}{T}}$, where L_{op} is the smoothness constant of f with respect to the
 249 operatorwnorm. Similarly, the best guarantee for BlockMuon is achieved by $\eta_{\text{block},*} = \sqrt{\frac{f(X_0) - f_*}{6TL_B}}$
 250 and is $B^*(\nabla f(X'_\tau)) \leq \sqrt{\frac{2L_B(f(X_0) - f_*)}{T}}$, where $\tau' = \arg \min_t B^*(\nabla f(X'_t))$ and L_B is the smoothness
 251 constant of f in the block norm $B(\cdot)$. To compare the two guarantees for BlockMuon and
 252 Muon, we use the facts that $\|\cdot\|_{\text{op},*} \leq B^*(\cdot)$ and $L_B \leq rcL_{\text{op}}$ (proved in Appendix A.1) to get
 253 $\|\nabla f(X'_{\tau'})\|_{\text{op},*} \leq \sqrt{\frac{2L_B(f(X_0) - f_*)}{T}} \leq \sqrt{rc}\sqrt{\frac{2L_{\text{op}}(f(X_0) - f_*)}{T}}$. Thus, under the same operator norm
 254 metric, BlockMuon's best point $X'_{\tau'}$ has a gradient dual norm that is at most a \sqrt{rc} factor worse than
 255 Muon's best point X_τ in the worst case; when $L_B \approx L_{\text{op}}$ (e.g., curvature well captured by blocks),
 256 the two bounds match up to constants. Note that in the former case, we would have $L_B \approx (rc)L_{\text{op}}$
 257 and $\frac{\eta_{\text{op},*}}{\eta_{\text{block},*}} = \sqrt{\frac{L_B}{L_{\text{op}}}} = \sqrt{rc}$. Whereas, in the ideal scenario when $\eta_{\text{op},*} \approx \eta_{\text{block},*}$, the optimal
 258 learning rate would be the same for both algorithms. Thus *the optimal ratio of the learning rate of*
 259 *Block-Muon and Muon is between 1 and $1/\sqrt{rc}$.*

264 The picture we see is thus clear: BlockMuon is faster on a per-step basis, as we do not need to
 265 perform any additional communication over coordinate-wise methods, but this comes at the cost
 266 of a worse convergence guarantee (by a factor of \sqrt{rc} in the worst case). It seems straightforward
 267 then that we should minimize wall-clock time by choosing block sizes r and c that balance this
 268 tradeoff. While this is theoretically plausible, in practice the block sizes are naturally a function of
 269 network topology (i.e. FSDP or TP degrees) and changing them would add more latency and require
 270 redistributing tensors to and from their original layouts.

270 3.2 BLOCK-PERIODIC ORTHOGONALIZATION
271

272 We instead offer another alternative to tuning block sizes that (a) has a simple implementation, and
273 (b) gives us a clear tunable knob that smoothly interpolates between BlockMuon and Muon. Given a
274 period P , Muon with Block-Periodic orthogonalization instead uses BlockMuon for $\frac{P-1}{P}$ steps and
275 then uses full orthogonalization for one step. If $P = 1$ we get Muon, while if $P \rightarrow \infty$ we get Block-
276 Muon. Using P in between both extremes allows us to balance out the tradeoff between iteration
277 complexity and per-step communication cost. We state the algorithm in full below as Algorithm 1.
278 Note that we use two stepsizes, η_{full} and η_{block} , depending on whether we communicate during that
279 step or not. We will later show this gives a better convergence rate than just using one stepsize.

280 The next theorem studies the convergence of this algorithm and allows us to make the above intuition
281 rigorous.

282 **Theorem 2** (Convergence of MuonBP). *Suppose that f satisfies Assumption 1 with respect to both
283 the operator norm $\|\cdot\|_{\text{op}}$ with constant L_{op} and the block-spectral norm $B(\cdot)$ with constant L_B ,
284 and that Assumption 2 holds. Assume f is lower bounded by f_* and let $\Delta_0 = f(X_0) - f_*$. Fix
285 a period $P \geq 1$, momentum $\mu \in [0, 1]$, and two stepsizes $\eta_{\text{full}} > 0$ and $\eta_{\text{block}} > 0$. Define
286 $\bar{\eta} = \frac{\eta_{\text{full}}}{P} + \frac{\eta_{\text{block}}(P-1)}{P}$, $\eta_{\text{max}} = \max(\eta_{\text{full}}, \eta_{\text{block}})$, and*

$$287 A = \max\{\eta_{\text{full}}\sqrt{L_{\text{op}}}, \eta_{\text{block}}\sqrt{L_B}\}, \quad Q = \frac{L_{\text{op}}\eta_{\text{full}}^2}{2P} + \frac{L_B\eta_{\text{block}}^2(P-1)}{2P},$$

$$288 R = \frac{2\mu}{1-\mu} \left(\frac{L_{\text{op}}\eta_{\text{full}} \max\{\eta_{\text{block}}\sqrt{rc}, \eta_{\text{full}}\}}{P} + \frac{L_B\eta_{\text{block}} \max\{\eta_{\text{full}}, \eta_{\text{block}}\}(P-1)}{P} \right).$$

289 Then for any horizon T divisible by P , the iterates of Algorithm 1 satisfy

$$290 \min_{t=0, \dots, T-1} \mathbb{E} [\|\nabla f(X_t)\|_{\text{op},*}] \leq \frac{\Delta_0}{\bar{\eta}T} + \frac{4(1-\mu)\sigma\eta_{\text{max}}}{\bar{\eta}T} + \frac{6\mu\sqrt{\Delta_0}A}{(1-\mu)\bar{\eta}T} + \frac{Q+R}{\bar{\eta}} + 2\sigma\sqrt{\frac{1-\mu}{1+\mu}}. \quad (4)$$

291 To simplify the comparison we consider the noiseless case where $\sigma = 0$ and the optimal momentum
292 parameter is then $\mu = 0$. To minimize Equation (4), we define the harmonic-average smoothness
293 \bar{L}_{BP} by $\bar{L}_{\text{BP}}^{-1} = \frac{1}{P}L_{\text{op}}^{-1} + \frac{P-1}{P}L_B^{-1}$. The optimal stepsizes are then $\eta_{\text{full}}^* = \frac{1}{L_{\text{op}}}\sqrt{\frac{2\Delta_0}{T}\bar{L}_{\text{BP}}}$ and
294 $\eta_{\text{block}}^* = \frac{1}{L_B}\sqrt{\frac{2\Delta_0}{T}\bar{L}_{\text{BP}}}$ and the convergence rate is $\min_{t < T} \|\nabla f(X_t)\|_{\text{op},*} \leq \sqrt{\frac{2\Delta_0\bar{L}_{\text{BP}}}{T}}$. Therefore,
295 the convergence of BlockMuon, Muon, and MuonBP is proportional to $\sqrt{L_B}$, $\sqrt{L_{\text{op}}}$, and
296 $\sqrt{\bar{L}_{\text{BP}}}$, respectively. It is easy to see that $L_{\text{op}} \leq \bar{L}_{\text{BP}} \leq L_B$ and thus the convergence rate of
297 MuonBP is in between Muon and BlockMuon. The period P acts as a tunable knob that lets us slide
298 between the two extremes and this is directly reflected in the convergence rates we obtain. Observe
299 that to get this rate, it is crucial that we use two stepsizes η_{full} and η_{block} depending on whether
300 we are applying full orthogonalization or block-wise orthogonalization. On the contrary, if we were
301 to force using a single stepsize for all steps $\eta_t \equiv \eta$, the optimal choice becomes $\eta^* = \sqrt{\frac{2\Delta_0}{T\bar{L}_{\text{BP}}}}$
302 with $\bar{L}_{\text{BP}} = \frac{L_{\text{op}}}{P} + \frac{P-1}{P}L_B$, yielding a convergence rate proportional to \bar{L}_{BP} rather than \bar{L}_{BP} .
303 Since \bar{L}_{BP} is the weighted harmonic mean and $\bar{L}_{\text{BP}} = \frac{L_{\text{op}} + (P-1)L_B}{P}$ is the weighted arithmetic mean of the same
304 constants, we have $\bar{L}_{\text{BP}} \leq \bar{L}_{\text{BP}} = \frac{L_{\text{op}} + (P-1)L_B}{P}$ with strict inequality unless $L_{\text{op}} = L_B$, so tying the stepsizes
305 generally yields worse convergence. Observe that, as in our previous comparison, the optimal ratio
306 between η_{block} and η_{full} is between 1 and $1/\sqrt{rc}$.

307 **AdamW learning rate transfer.** Liu et al. (2025) introduce a learning rate scaling rule that allows
308 reusing the AdamW learning rate for Muon by matching the root-mean square norm of the updates
309 to be the same as AdamW. To ensure that the updates have RMS β , they scale the update matrices
310 by $\beta \cdot \sqrt{\max(m, n)}$ where $m \times n$ are the update matrix dimensions. Following our theorem above,
311 which shows using different learning rates for the blocking and non-blocking matrices is ideal, we
312 also adopt this rule and scale the updates by the dimensions of the smaller matrix on block steps and
313 the dimensions of the full matrix on non-blocking steps.

314 **Communication cost of MuonBP.** On a *block* step, MuonBP performs orthogonalization on the
315 local shard and updates the local parameter slice; no optimizer-state all-gather/scatter is needed.
316 Only the usual DP gradient all-reduce (already required by the training stack) occurs. On a *full*
317 step, MuonBP temporarily gathers shards to materialize M_t (or G_t) per tensor, performs global
318 orthogonalization, then scatters back.

324
 325 **Algorithm 1:** MuonBP
 326 1 $M_{-1}^{(m)} \leftarrow 0$ for all devices m
 327 2 **for** $t \leftarrow 0$ **to** $T - 1$ **do**
 328 3 **for** each device m **do in parallel**
 329 4 Get local shard $G_t^{(m)}$ of the full
 330 gradient G_t
 331 5 $M_t^{(m)} \leftarrow \mu M_{t-1}^{(m)} + G_t^{(m)}$
 332 6 **if** $t \bmod P = 0$ **then**
 333 7 Gather $\{M_t^{(m)}\}_m$ to form full M_t
 334 8 $U_t \leftarrow \text{Orthogonalize-via-NS}(M_t)$
 335 9 $X_{t+1} \leftarrow X_t - \eta_{\text{full}} U_t$
 336 10 **else**
 337 11 **for** each device m **do in parallel**
 338 12 $U_t^{(m)} \leftarrow$
 339 Orthogonalize-via-NS($M_t^{(m)}$)
 340 $X_{t+1}^{(m)} \leftarrow X_t^{(m)} - \eta_{\text{block}} U_t^{(m)}$
 341 13 **return** X_T

342
 343
 344
 345
 346 method with a small 160M model setup from (Ahn et al., 2025); and compare MuonBP to AdamW, Muon (with full all-gather at every step), BlockMuon, and Dion. FSDP2 shards optimizer states in 0th dimension to different workers, resulting in increased communication for Muon. In the second setting we use ZeRO layer-wise (Rajbhandari et al., 2019) optimizer state sharding and TP. Here, we primarily compare MuonBP (Algorithm 1), BlockMuon (Algorithm 1 with $P = \infty$), and baseline Muon (with full all-gather every step), under billion scale model sizes and longer tokens. Both experiment groups are meant to showcase the accuracy and throughput improvements brought about by our algorithm in realistic pretraining settings.

354
 355 4.1 TRAINING WITH DIM-0 DATA SHARDING

356
 357 **Experimental setting and hyperparameters.** We augment
 358 the Modded-NanoGPT codebase (Jordan et al.,
 359 2024a) with SimpleFSDP (Zhang et al., 2024) and
 360 TP (Shoeybi et al., 2019) via the DTensor API integrated
 361 into PyTorch 2.0 (Liang, 2023). We use the **FineWeb**
 362 dataset (Penedo et al., 2024) for the experiments in this
 363 section.

364 Figure 1 shows the effect of varying both the TP degree
 365 and the period of orthogonalization on the final validation
 366 loss achieved. We use the modernized GPT-style archi-
 367 tecture of Modded-NanoGPT (Jordan et al., 2024a) for
 368 this experiment. We use 12 layers, 6 attention heads, and
 369 a model dimension of 768. We use the smaller model
 370 size (280M) in order to run an extensive grid search. Fol-
 371 lowing the codebase, we use separate learning rates for
 372 Adam (applied to 1D parameters and the input embed-
 373 ding) and Muon, and do not use the RMS norm matching
 374 trick of Section 4.2. We tune the Adam/Muon learning
 375 rates over the grid $(0.0001, 0.001, 0.01, 0.1, 0.5, 1, 2, 4, 8) * \text{base}$ where $\text{base} = 0.012$ for Adam
 376 and $\text{base} = 0.08$ for Muon. We see that decreasing the block period directly decreases the loss for
 377 all the degrees we consider, with the effect most pronounced at the highest degrees.

378 We use the Dion codebase (Ahn et al., 2025) for the second comparison and train a 160M pa-
 379 rameter model with a batch size of 1024, sequence length 1024, model dimension 768, 12 layers

Choice of period. Ideally the period P should be chosen to minimize the wall-clock time to reach a certain accuracy ε , defined as the product of number of iterations to reach this accuracy $T_{\text{iter}}(\varepsilon, P)$ (which can be derived from Theorem 2) and the expected wall-clock time per iteration $T_{\text{wall}}(P)$. The latter is a function of network communication speed, the model parallelism used, and tensor dimensions. This can be difficult to model in closed form, and in practice we resort to trying out different values of P for shorter runs first. We found that the simple choice $P = 5$ balanced this tradeoff well in most of our experiments.

4 EXPERIMENTS

We conduct experiments in two main settings both of which are Llama-style language model pretraining setups. Firstly, we use a setting with FSDP2 and TP where we study the effect of varying blocking degree and orthogonalization period on convergence under extensive hyperparameter tuning. Then, we benchmark our

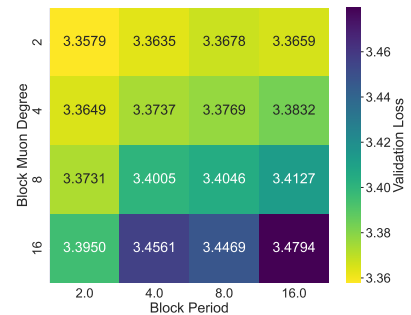


Figure 1: Validation loss as a function of orthogonalization period for different TP degrees (280M model).

378 and 12 attention heads per attention layer. We use the WSD schedule with no warmup and a 20%
 379 cooldown. The learning rate is 0.02 for all methods (with AdamW rms norm matching) except for
 380 AdamW, where we found by a grid search that 0.008 performed better. We use TP degree of 2 and
 381 FSDP degree of 4, and use Lion as the scalar optimizer in line with the codebase. The throughputs
 382 for all the methods were similar at this scale, although they were significantly lower compared to
 383 throughputs on Megatron-LM with layerwise sharding. We believe more experiments are needed to
 384 compare against Dion, particularly to integrate it into widely used open source frameworks such as
 385 Megatron-LM. We also plot the loss curves in Figure 11 in Appendix B.

	Muon	BlockMuon	MuonBP	Dion	AdamW
Min Validation Loss	3.36	3.36	3.34	3.37	3.62
Min Training Loss	3.02	2.97	2.94	2.95	3.21
Throughput (TFLOP/s/GPU)	50.90	51.77	51.40	45.64	52.80

392 Table 1: Training/validation losses and throughput on 160M model trained with TP=2 and FSDP=4.
 393

394 4.2 TRAINING WITH LAYERWISE-SHARDING

397 **Experimental setting and hyperparameters.** We built upon the Distributed Muon implemen-
 398 tation of (Liu et al., 2025) in the Megatron-LM framework (Shoeybi et al., 2019) and mod-
 399 ified it to support block-wise tensor parallel orthogonalization with periodic full orthogonal-
 400 ization. We used Llama-style model architecture (Touvron et al., 2023a;b) with RoPE (Su
 401 et al., 2024), SwiGLU activation (Shazeer, 2020), and mixed-precision training (bf16 computa-
 402 tions with fp32 master weights). We use the Llama 3 tokenizer (Grattafiori et al., 2024)
 403 on the **OpenWebText** dataset (Gokaslan et al., 2019) for experiments at the 0.9-1.2B scale
 404 and the **FineWeb** data (Penedo et al., 2024) for experiments at the 8B scale. For the ex-
 405 periments in this section, we used nodes that have 8xA100 GPUs with 40GB of RAM each.
 406

407 We train models in the following scales and settings: 960M and
 408 1.26B, 1.26B with extended training (3x Chinchilla tokens), and 8B
 409 parameters with large (1.2×10^{-3}) and small (0.6×10^{-3}) learn-
 410 ing rates. The models below 8B in scale use a batch size of 128
 411 sequences and each run takes place on a single node with 2 DP
 412 groups and 4 TP nodes per group. The 8B model uses a batch size
 413 of 256 sequences with 4 DP groups distributed across 4 nodes and
 414 8 TP nodes per group. As discussed in Section 3.2, we use AdamW
 415 RMS norm matching for learning rate scaling (Liu et al., 2025). All
 416 of the architectural details are provided in Table 4 in the supple-
 417 mentary material and more details on our choices of hyperparam-
 418 eters, learning rate, and learning rate scheduling are found in the
 419 appendix. We do the two learning rate runs at 8B scale to show that
 420 with the larger base learning rate, even after adjusting for blocking
 with the RMS norm matching, BlockMuon becomes unstable.

421 **Results.** Resulting perplexities are summarized in Table 2. The loss curves for all models are
 422 deferred to Appendix B. Table 2 shows that BlockMuon performs worse in both training and vali-
 423 dation loss across all model scales considered. This still holds true for relatively long (3x Chinchilla)
 424 training, as the parameter norms grow a lot more for the fully blocked version of Muon compared
 425 to either baseline or blocking with intermittent orthogonalization. Note that this happens despite
 426 the fact that we use AdamW RMS norm matching scaled with the dimensions of the sliced blocks
 427 (as outlined in Section Section 3). We observe that we have to use smaller learning rates to keep
 428 BlockMuon stable compared to Muon and MuonBP and is potentially a symptom of the instability
 429 we observe when using BlockMuon. We do not observe instability when using smaller learning rates
 430 (Figure 10), but then baseline Muon, BlockMuon, and MuonBP all lead to the same suboptimal per-
 431 formance. In Figure 3, we plot the validation ppl vs wall-clock time. We characterize our method’s
 432 performance with respect to two related metric: firstly, given a target ppl value our method reaches
 433 considerably faster in wall-clock time; secondly given a runtime budget our method results in lower

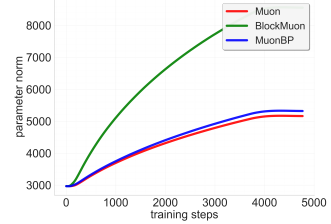


Figure 2: Parameter norm vs
 iteration of competing meth-
 ods.

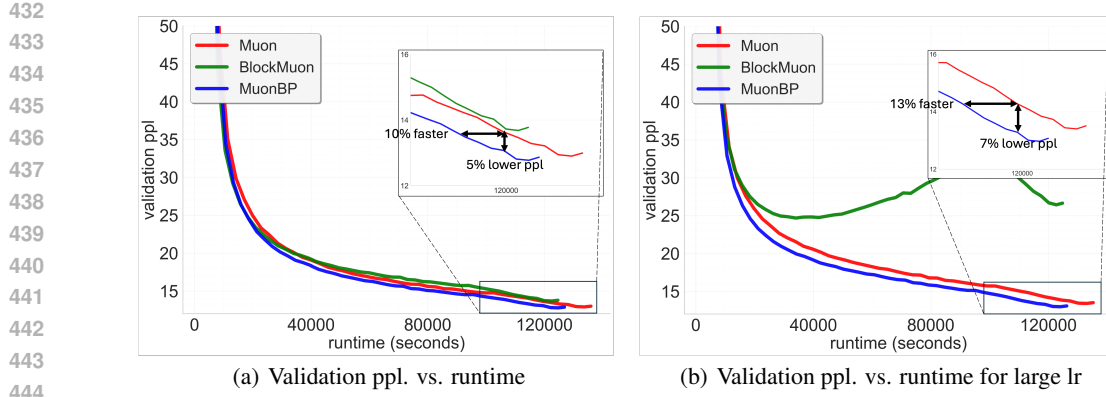


Figure 3: 8B model validation perplexities. Comparison of Muon, BlockMuon, and MuonBP across wall-clock time. For a target validation perplexity our method is $\sim 10 - 13\%$ faster in terms of the wall-clock time to reach it, and for a given time point before the learning rate decay our method results in $\sim 5 - 7\%$ lower perplexity compared to the baseline.

Table 2: Validation and training perplexity (*lower is better*). Columns show models; each model has validation and training sub-columns. Best perplexities within each model size are in **bold**.

Method	960M		1.2B		1.2B ^a		8B		8B ^b	
	Val	Train	Val	Train	Val	Train	Val	Train	Val	Train
Muon	15.33	13.44	14.13	12.83	12.62	10.88	12.90	11.74	13.40	12.39
BlockMuon	20.29	18.08	16.28	14.86	13.29	11.51	13.68	12.62	24.68	23.17
MuonBP	15.12	13.21	13.78	12.44	12.45	10.71	12.77	11.59	12.97	11.93

^aThree-times data with large learning rate. ^bLarge learning rate.

validation ppl (we give exemplary points in Figure 3). These two views indicate the usefulness of MuonBP in practical scenarios.

Interestingly, overall, our method outperforms Muon despite doing less number of full orthogonalization, we believe this may be due to a regularization effect due to intermittency, we leave the analysis of this behavior as future work.

Throughput. We report throughput numbers in table 3. We observe similar throughput across methods in smaller scale experiments as layer-wise sharding results in minimal all-gathers for the Muon. However, as the model scale increases the effect of all-gathers makes its presence felt. Consequently, in 8B model setting we observe a $\sim 8\%$ increase in throughput for our method compared to the Muon without any degradation in performance. This translates to hundreds of thousands of dollars saved in training costs in today’s large-scale pretraining runs.

5 CONCLUSION

We have introduced a new algorithm, MuonBP, and analyzed its convergence properties. MuonBP shows promising performance in training models up to the 8B parameter scale compared to Muon and BlockMuon. There are many questions still left: for example, we did not explore varying the period P over the duration of training, or how we might adaptively tune it based on observed properties. Exploring the use of block orthogonalization with expert parallelism is also an important topic we leave to future work.

Table 3: Average throughput (TFLOP/s/GPU) for each method and model.

Method	960M	1.2B	8B
Muon	112.97	136.53	105.09
BlockMuon	115.43	139.17	114.75
MuonBP	113.54	138.95	113.37

486 REPRODUCIBILITY STATEMENT
487

488 Section 3 and the Appendix provide all details necessary to reproduce the theoretical results
489 presented in this paper. Our code-base is built upon publicly available frameworks (Megatron-
490 LM (Shoeybi et al., 2019) and Modded NanoGPT (Jordan et al., 2024a)). Section 4 and the Ap-
491 pendix describe the experimental settings and hyperparameters in detail. To further support repro-
492 ductibility, we will release our implementation and training scripts upon publication.

494 REFERENCES
495

496 Kwangjun Ahn, Byron Xu, Natalie Abreu, and John Langford. Dion: Distributed orthonormalized
497 updates. *arXiv preprint arXiv:2504.05295*, 2025. URL <http://arxiv.org/abs/2504.05295v2>.

498 Joshua Ainslie, James Lee-Thorp, Michiel de Jong, Yury Zemlyanskiy, Federico Lebrón, and Sumit
499 Sanghali. GQA: Training generalized multi-query transformer models from multi-head check-
500 points. In Houda Bouamor, Juan Pino, and Kalika Bali (eds.), *Proceedings of the 2023 Conference*
501 *on Empirical Methods in Natural Language Processing*, pp. 4895–4901, Singapore, December
502 2023. Association for Computational Linguistics. doi: 10.18653/v1/2023.emnlp-main.298. URL
503 <https://aclanthology.org/2023.emnlp-main.298/>.

504 Noah Amsel, David Persson, Christopher Musco, and Robert M. Gower. The polar express:
505 Optimal matrix sign methods and their application to the Muon algorithm. *arXiv preprint*
506 *arXiv:2505.16932*, 2025. URL <http://arxiv.org/abs/2505.16932v2>.

507 Kang An, Yuxing Liu, Rui Pan, Yi Ren, Shiqian Ma, Donald Goldfarb, and Tong Zhang. ASGO:
508 Adaptive structured gradient optimization. *arXiv preprint arXiv:2503.20762*, 2025. URL <http://arxiv.org/abs/2503.20762v2>.

509 Jeremy Bernstein. Deriving Muon, 2025. URL <https://jeremybernste.in/writing/deriving-muon>.

510 Jeremy Bernstein and Laker Newhouse. Modular duality in deep learning. *arXiv preprint*
511 *arXiv:2410.21265*, 2024a. URL <http://arxiv.org/abs/2410.21265v2>.

512 Jeremy Bernstein and Laker Newhouse. Old optimizer, new norm: an anthology. *arXiv preprint*,
513 abs/2409.20325, 2024b. URL <https://arXiv.org/abs/2409.20325>.

514 Valentyn Boreiko, Zhiqi Bu, and Sheng Zha. Towards understanding of orthogonalization in muon.
515 In *High-dimensional Learning Dynamics 2025*, 2025. URL <https://openreview.net/forum?id=ppmyFtr9EW>.

516 Essential AI. Layer sharding for large-scale training with Muon. Essential AI Blog, May 2025.
517 URL <https://www.essential.ai/blog/infra>.

518 Essential AI, Ishaan Shah, Anthony M. Polloreno, Karl Stratos, Philip Monk, Adarsh Chaluvaraju,
519 Andrew Hojel, Andrew Ma, Anil Thomas, Ashish Tanwer, Darsh J Shah, Khoi Nguyen, Kurt
520 Smith, Michael Callahan, Michael Pust, Mohit Parmar, Peter Rushton, Platon Mazarakis, Ritvik
521 Kapila, Saurabh Srivastava, Somanshu Singla, Tim Romanski, Yash Vanjani, and Ashish Vaswani.
522 Practical efficiency of Muon for pretraining. *arXiv preprint arXiv:2505.02222*, 2025.

523 Athanasios Glentis, Jiaxiang Li, Andi Han, and Mingyi Hong. A minimalist optimizer design for
524 LLM pretraining. *arXiv preprint arXiv:2506.16659*, 2025. URL <http://arxiv.org/abs/2506.16659v1>.

525 Aaron Gokaslan, Vanya Cohen, Ellie Pavlick, and Stefanie Tellex. OpenWebText corpus. <http://Skylion007.github.io/OpenWebTextCorpus>, 2019.

526 Aaron Grattafiori, Abhimanyu Dubey, Abhinav Jauhri, Abhinav Pandey, Abhishek Kadian, Ahmad
527 Al-Dahle, Aiesha Letman, Akhil Mathur, Alan Schelten, Alex Vaughan, et al. The llama 3 herd
528 of models. *arXiv preprint arXiv:2407.21783*, 2024.

540 Vineet Gupta, Tomer Koren, and Yoram Singer. Shampoo: Preconditioned stochastic tensor opti-
 541 mization. *CoRR*, 2018. URL <http://arxiv.org/abs/1802.09568v2>.

542

543 Alex Hägele, Elie Bakouch, Atli Kosson, Leandro Von Werra, and Martin Jaggi. Scaling laws
 544 and compute-optimal training beyond fixed training durations. *Advances in Neural Information
 545 Processing Systems*, 37:76232–76264, 2024.

546 Yanping Huang, Youlong Cheng, Ankur Bapna, Orhan Firat, Mia Xu Chen, Dehao Chen, Hy-
 547 oukJoong Lee, Jiquan Ngiam, Quoc V. Le, Yonghui Wu, and Zhifeng Chen. GPipe: Effi-
 548 cient training of giant neural networks using pipeline parallelism. *CoRR*, 2018. URL <http://arxiv.org/abs/1811.06965v5>.

549

550 Keller Jordan, Jeremy Bernstein, Brendan Rappazzo, fernbear.bsky.social, Boza Vlado, You Ji-
 551 acheng, Franz Cesista, Braden Koszarsky, and Grad62304977. modded-nanopt: Speedrun-
 552 ning the nanopt baseline, 2024a. URL <https://github.com/KellerJordan/modded-nanopt>.

553

554 Keller Jordan, Yuchen Jin, Vlado Boza, Jiacheng You, Franz Cesista, Laker Newhouse, and Jeremy
 555 Bernstein. Muon: An optimizer for hidden layers in neural networks, 2024b. URL <https://kellerjordan.github.io/posts/muon/>.

556

557 Diederik P. Kingma and Jimmy Ba. Adam: A method for stochastic optimization. In Yoshua
 558 Bengio and Yann LeCun (eds.), *3rd International Conference on Learning Representations, ICLR
 559 2015, San Diego, CA, USA, May 7-9, 2015, Conference Track Proceedings*, 2015. URL <http://arXiv.org/abs/1412.6980>.

560

561 Dmitry Kovalev. Understanding gradient orthogonalization for deep learning via non-euclidean
 562 trust-region optimization. *CoRR*, 2025. URL <http://arxiv.org/abs/2503.12645v2>.

563

564 Jiaxiang Li and Mingyi Hong. A note on the convergence of muon. *arXiv preprint
 565 arXiv:2502.02900*, 2025.

566

567 Wanchao Liang. Pytorch dtensor rfc. GitHub Issue, 2023. URL <https://github.com/pytorch/pytorch/issues/88838>. GitHub Issue #88838.

568

569 Wanchao Liang, Tianyu Liu, Less Wright, Will Constable, Andrew Gu, Chien-Chin Huang, Iris
 570 Zhang, Wei Feng, Howard Huang, Junjie Wang, Sanket Purandare, Gokul Nadathur, and Stratos
 571 Idreos. TorchTitan: One-stop pytorch native solution for production ready LLM pre-training.
 572 *CoRR*, 2024. URL <http://arxiv.org/abs/2410.06511v1>.

573

574 Jingyuan Liu, Jianlin Su, Xingcheng Yao, Zhejun Jiang, Guokun Lai, Yulun Du, Yidao Qin, Weixin
 575 Xu, Enzhe Lu, Junjie Yan, Yanru Chen, Huabin Zheng, Yibo Liu, Shaowei Liu, Bohong Yin,
 576 Weiran He, Han Zhu, Yuzhi Wang, Jianzhou Wang, Mengnan Dong, Zheng Zhang, Yongsheng
 577 Kang, Hao Zhang, Xinran Xu, Yutao Zhang, Yuxin Wu, Xinyu Zhou, and Zhilin Yang. Muon is
 578 scalable for LLM training. *CoRR*, 2025. URL <http://arxiv.org/abs/2502.16982v1>.

579

580 Ilya Loshchilov and Frank Hutter. Decoupled weight decay regularization. In *7th International
 581 Conference on Learning Representations, ICLR 2019, New Orleans, LA, USA, May 6-9, 2019.
 582 OpenReview.net*, 2019a. URL <https://openreview.net/forum?id=Bkg6RiCqY7>.

583

584 Ilya Loshchilov and Frank Hutter. Decoupled weight decay regularization. In *International Confer-
 585 ence on Learning Representations*, 2019b. URL <https://openreview.net/forum?id=Bkg6RiCqY7>.

586

587 James Martens and Roger Grosse. Optimizing neural networks with kronecker-factored approximate
 588 curvature. In *International conference on machine learning*, pp. 2408–2417. PMLR, 2015.

589

590 Guilherme Penedo, Hynek Kydlíček, Anton Lozhkov, Margaret Mitchell, Colin A Raffel, Leandro
 591 Von Werra, Thomas Wolf, et al. The fineweb datasets: Decanting the web for the finest text data
 592 at scale. *Advances in Neural Information Processing Systems*, 37:30811–30849, 2024.

593

594 Thomas Pethick, Wanyun Xie, Kimon Antonakopoulos, Zhenyu Zhu, Antonio Silveti-Falls, and
 595 Volkan Cevher. Training deep learning models with norm-constrained lmos. *CoRR*, 2025. URL
<http://arxiv.org/abs/2502.07529v2>.

594 Samyam Rajbhandari, Jeff Rasley, Olatunji Ruwase, and Yuxiong He. ZeRO: Memory optimizations
 595 toward training trillion parameter models. *CoRR*, 2019. URL <http://arxiv.org/abs/1910.02054v3>.

597 Noam Shazeer. GLU variants improve transformer, 2020. URL <https://arxiv.org/abs/2002.05202>.

600 Hao-Jun Michael Shi, Tsung-Hsien Lee, Shintaro Iwasaki, Jose Gallego-Posada, Zhijing Li,
 601 Kaushik Rangadurai, Dheevatsa Mudigere, and Michael Rabbat. A distributed data-parallel py-
 602 torch implementation of the distributed shampoo optimizer for training neural networks at-scale.
 603 *CoRR*, 2023. URL <http://arxiv.org/abs/2309.06497v1>.

604 Mohammad Shoeybi, Mostofa Patwary, Raul Puri, Patrick LeGresley, Jared Casper, and Bryan
 605 Catanzaro. Megatron-lm: Training multi-billion parameter language models using model par-
 606 allelism. *arXiv preprint arXiv:1909.08053*, 2019.

607 Jianlin Su, Murtadha Ahmed, Yu Lu, Shengfeng Pan, Wen Bo, and Yunfeng Liu. RoFormer: En-
 609 hanced transformer with rotary position embedding. *Neurocomputing*, 568:127063, 2024.

610 Kimi Team, Yifan Bai, Yiping Bao, Guanduo Chen, Jiahao Chen, Ningxin Chen, Ruijue Chen,
 611 Yanru Chen, Yuankun Chen, Yutian Chen, Zhuofu Chen, Jialei Cui, Hao Ding, Mengnan Dong,
 612 Angang Du, Chenzhuang Du, Dikang Du, Yulun Du, Yu Fan, Yichen Feng, Kelin Fu, Bofei Gao,
 613 Hongcheng Gao, Peizhong Gao, Tong Gao, Xinran Gu, Longyu Guan, Haiqing Guo, Jianhang
 614 Guo, Hao Hu, Xiaoru Hao, Tianhong He, Weiran He, Wenyang He, Chao Hong, Yangyang Hu,
 615 Zhenxing Hu, Weixiao Huang, Zhiqi Huang, Zihao Huang, Tao Jiang, Zhejun Jiang, Xinyi Jin,
 616 Yongsheng Kang, Guokun Lai, Cheng Li, Fang Li, Haoyang Li, Ming Li, Wentao Li, Yanhao
 617 Li, Yiwei Li, Zhaowei Li, Zheming Li, Hongzhan Lin, Xiaohan Lin, Zongyu Lin, Chengyin
 618 Liu, Chenyu Liu, Hongzhang Liu, Jingyuan Liu, Junqi Liu, Liang Liu, Shaowei Liu, T. Y. Liu,
 619 Tianwei Liu, Weizhou Liu, Yangyang Liu, Yibo Liu, Yiping Liu, Yue Liu, Zhengying Liu, Enzhe
 620 Lu, Lijun Lu, Shengling Ma, Xinyu Ma, Yingwei Ma, Shaoguang Mao, Jie Mei, Xin Men, Yibo
 621 Miao, Siyuan Pan, Yebo Peng, Ruoyu Qin, Bowen Qu, Zeyu Shang, Lidong Shi, Shengyuan Shi,
 622 Feifan Song, Jianlin Su, Zhengyuan Su, Xinjie Sun, Flood Sung, Heyi Tang, Jiawen Tao, Qifeng
 623 Teng, Chensi Wang, Dinglu Wang, Feng Wang, Haiming Wang, Jianzhou Wang, Jiaxing Wang,
 624 Jinhong Wang, Shengjie Wang, Shuyi Wang, Yao Wang, Yejie Wang, Yiqin Wang, Yuxin Wang,
 625 Yuzhi Wang, Zhaoji Wang, Zhengtao Wang, Zhexu Wang, Chu Wei, Qianqian Wei, Wenhao Wu,
 626 Xingzhe Wu, Yuxin Wu, Chenjun Xiao, Xiaotong Xie, Weimin Xiong, Boyu Xu, Jing Xu, Jinjing
 627 Xu, L. H. Xu, Lin Xu, Suting Xu, Weixin Xu, Xinran Xu, Yangchuan Xu, Ziyao Xu, Junjie
 628 Yan, Yuzi Yan, Xiaofei Yang, Ying Yang, Zhen Yang, Zhilin Yang, Zonghan Yang, Haotian Yao,
 629 Xingcheng Yao, Wenjie Ye, Zhuorui Ye, Bohong Yin, Longhui Yu, Enming Yuan, Hongbang
 630 Yuan, Mengjie Yuan, Haobing Zhan, Dehao Zhang, Hao Zhang, Wanlu Zhang, Xiaobin Zhang,
 631 Yangkun Zhang, Yizhi Zhang, Yongting Zhang, Yu Zhang, Yutao Zhang, Yutong Zhang, Zheng
 632 Zhang, Haotian Zhao, Yikai Zhao, Huabin Zheng, Shaojie Zheng, Jianren Zhou, Xinyu Zhou,
 633 Zaida Zhou, Zhen Zhu, Weiyu Zhuang, and Xinxing Zu. Kimi K2: Open agentic intelligence.
 634 *arXiv preprint arXiv:2507.20534*, 2025. URL <https://arxiv.org/abs/2507.20534>.

635 Hugo Touvron, Thibaut Lavril, Gautier Izacard, Xavier Martinet, Marie-Anne Lachaux, Timothée
 636 Lacroix, Baptiste Rozière, Naman Goyal, Eric Hambro, Faisal Azhar, Aurelien Rodriguez, Ar-
 637 mand Joulin, Edouard Grave, and Guillaume Lample. Llama: Open and efficient foundation
 638 language models. *arXiv preprint abs/2302.13971*, 2023a. URL <https://arxiv.org/abs/2302.13971>.

639 Hugo Touvron, Louis Martin, Kevin Stone, Peter Albert, Amjad Almahairi, Yasmine Babaei, Niko-
 640 lay Bashlykov, Soumya Batra, Prajjwal Bhargava, Shruti Bhosale, Dan Bikel, Lukas Blecher,
 641 Cristian Canton Ferrer, Moya Chen, Guillem Cucurull, David Esiobu, Jude Fernandes, Jeremy
 642 Fu, Wenyin Fu, Brian Fuller, Cynthia Gao, Vedanuj Goswami, Naman Goyal, Anthony Hartshorn,
 643 Saghar Hosseini, Rui Hou, Hakan Inan, Marcin Kardas, Viktor Kerkez, Madian Khabsa, Isabel
 644 Kloumann, Artem Korenev, Punit Singh Koura, Marie-Anne Lachaux, Thibaut Lavril, Jenya Lee,
 645 Diana Liskovich, Yinghai Lu, Yuning Mao, Xavier Martinet, Todor Mihaylov, Pushkar Mishra,
 646 Igor Molybog, Yixin Nie, Andrew Poulton, Jeremy Reizenstein, Rashi Rungta, Kalyan Saladi,
 647 Alan Schelten, Ruan Silva, Eric Michael Smith, Ranjan Subramanian, Xiaoqing Ellen Tan, Binh
 Tang, Ross Taylor, Adina Williams, Jian Xiang Kuan, Puxin Xu, Zheng Yan, Iliyan Zarov, Yuchen

648 Zhang, Angela Fan, Melanie Kambadur, Sharan Narang, Aurelien Rodriguez, Robert Stojnic,
649 Sergey Edunov, and Thomas Scialom. Llama 2: Open foundation and fine-tuned chat models.
650 *arXiv preprint*, abs/2307.09288, 2023b. URL <https://arXiv.org/abs/2307.09288>.

651

652 Shuo Xie, Tianhao Wang, Sashank Reddi, Sanjiv Kumar, and Zhiyuan Li. Structured preconditioners
653 in adaptive optimization: a unified analysis. *CoRR*, 2025. URL <http://arxiv.org/abs/2503.10537v1>.

654

655 Ruiqi Zhang, Tianyu Liu, Will Feng, Andrew Gu, Sanket Purandare, Wanchao Liang, and Francisco
656 Massa. SimpleFSDP: Simpler fully sharded data parallel with torch.compile, 2024. URL <https://arxiv.org/abs/2411.00284>.

657

658 Yanli Zhao, Andrew Gu, Rohan Varma, Liang Luo, Chien-Chin Huang, Min Xu, Less Wright,
659 Hamid Shojanazeri, Myle Ott, Sam Shleifer, Alban Desmaison, Can Balioglu, Pritam Damania,
660 Bernard Nguyen, Geeta Chauhan, Yuchen Hao, Ajit Mathews, and Shen Li. Pytorch FSDP:
661 Experiences on scaling fully sharded data parallel. *CoRR*, 2023. URL <http://arxiv.org/abs/2304.11277v2>.

662

663

664

665

666

667

668

669

670

671

672

673

674

675

676

677

678

679

680

681

682

683

684

685

686

687

688

689

690

691

692

693

694

695

696

697

698

699

700

701

702 703 704 Appendix

705 A MAIN PROOFS

707 A.1 NORM EQUIVALENCES

709 **Lemma 2** (Dual of the block-spectral norm). *Let $X \in \mathbb{R}^{m \times n}$ be partitioned into $r \times c$ blocks
710 $X_{ij} \in \mathbb{R}^{m_b \times n_b}$ (not necessarily square). Define*

$$711 \quad B(X) = \max_{1 \leq i \leq r, 1 \leq j \leq c} \|X_{ij}\|_{\text{op}}.$$

713 *With the Frobenius inner product $\langle X, G \rangle = \text{tr}(X^\top G) = \sum_{i,j} \text{tr}(X_{ij}^\top G_{ij})$, one has*

$$715 \quad \sup_{B(G) \leq 1} \langle X, G \rangle = \sum_{i=1}^r \sum_{j=1}^c \|X_{ij}\|_*.$$

718 *Moreover, if $X_{ij} = U_{ij}\Sigma_{ij}V_{ij}^\top$ is an SVD, then*

$$720 \quad Z_{ij}^* = \begin{cases} U_{ij}V_{ij}^\top, & X_{ij} \neq 0, \\ 0, & X_{ij} = 0, \end{cases}$$

722 *is feasible with $B(Z^*) \leq 1$ and attains the supremum:*

$$724 \quad \langle X, Z^* \rangle = \sum_{i,j} \|X_{ij}\|_*.$$

726 *Consequently the dual norm of $B(\cdot)$ is $B^*(Y) = \sum_{i,j} \|Y_{ij}\|_*$.*

728 *Proof.* For any feasible G with $B(G) \leq 1$, Cauchy-Schwartz gives us

$$730 \quad \langle X_{ij}, G_{ij} \rangle \leq \|X_{ij}\|_* \|G_{ij}\|_{\text{op}} \leq \|X_{ij}\|_*.$$

732 Summing over blocks,

$$733 \quad \langle X, G \rangle = \sum_{i,j} \langle X_{ij}, G_{ij} \rangle \leq \sum_{i,j} \|X_{ij}\|_*.$$

735 Taking the supremum over feasible G yields

$$737 \quad \sup_{B(G) \leq 1} \langle X, G \rangle \leq \sum_{i,j} \|X_{ij}\|_*.$$

740 We now show the above upper bound is achieved by Z^* . Let $X_{ij} = U_{ij}\Sigma_{ij}V_{ij}^\top$ be an SVD and
741 define Z^* blockwise by $Z_{ij}^* = U_{ij}V_{ij}^\top$ if $X_{ij} \neq 0$ and $Z_{ij}^* = 0$ otherwise. Then $\|Z_{ij}^*\|_{\text{op}} = 1$ when
742 $X_{ij} \neq 0$ and 0 when $X_{ij} = 0$, so $B(Z^*) \leq 1$. Moreover,

$$744 \quad \langle X_{ij}, Z_{ij}^* \rangle = \text{tr}((U_{ij}\Sigma_{ij}V_{ij}^\top)^\top (U_{ij}V_{ij}^\top)) = \text{tr}(\Sigma_{ij}) = \|X_{ij}\|_*.$$

745 Summing over blocks gives $\langle X, Z^* \rangle = \sum_{i,j} \|X_{ij}\|_*$, which matches the upper bound, hence Z^*
746 is optimal and the stated supremum value holds. \square

748 **Lemma 3.** *The norm equivalence constants in Assumption 3 for the operator norm and block-
749 spectral norm are both equal to one. That is,*

$$750 \quad \rho_{\text{op}} = 1 \quad \text{and} \quad \rho_{\text{block}} = 1.$$

752 *Proof.* The operator norm $\|X\|_{\text{op}}$ (the largest singular value) is always less than or equal to
753 the Frobenius norm $\|X\|_F$ (the root-sum-square of all singular values), hence $\rho_{\text{op}} = 1$. The
754 block-spectral norm is a maximum of block operator norms, $B(X) = \max_{i,j} \|X_{ij}\|_{\text{op}} \leq$
755 $\max_{i,j} \|X_{ij}\|_F \leq \sqrt{\sum_{i,j} \|X_{ij}\|_F^2} = \|X\|_F$, which implies $\rho_{\text{block}} = 1$ as well. \square

756 **Lemma 4.** (Relations of norms) Suppose that $B(\cdot)$ is the block-norm corresponds to a partitioning
 757 a matrix of size $m \times n$ into $r \times c$ blocks of size $m_b \times n_b$ each. Then the following relations hold
 758

$$759 \quad B(G) \leq \|G\|_{\text{op}} \leq \sqrt{rc}B(G), \\ 760 \quad \|G\|_{\text{op},*} \leq B^*(G) \leq \sqrt{rc}\|G\|_{\text{op},*}.$$

761 Moreover, if a function f is L_{op} -smooth with respect to the operator norm and L_B -smooth with
 762 respect to the block-norm, we have

$$763 \quad L_{\text{op}} \leq L_B \leq (rc) \cdot L_{\text{op}}. \\ 764$$

765 *Proof.* Write G as an $r \times c$ block matrix with blocks $G_{ij} \in \mathbb{R}^{m_b \times n_b}$ and recall $B(G) =$
 766 $\max_{i,j} \|G_{ij}\|_{\text{op}}$. We first prove that $B(G) \leq \|G\|_{\text{op}}$. Let $R_i \in 0, 1^{m_b \times m}$ select the i -th block
 767 of rows and $C_j \in 0, 1^{n \times n_b}$ select the j -th block of columns, so $G_{ij} = R_i G C_j$. Because R_i and C_j
 768 are partial isometries, $\|R_i\|_{\text{op}} = \|C_j\|_{\text{op}} = 1$. By submultiplicativity,
 769

$$770 \quad \|G_{ij}\|_{\text{op}} = \|R_i G C_j\|_{\text{op}} \leq \|R_i\|_{\text{op}} \|G\|_{\text{op}} \|C_j\|_{\text{op}} = \|G\|_{\text{op}}.$$

771 Taking the maximum over (i, j) yields $B(G) \leq \|G\|_{\text{op}}$.

772 Now we prove the upper bound on $\|G\|_{\text{op}}$. Let $u \in \mathbb{R}^m$, $v \in \mathbb{R}^n$ be unit vectors and partition them
 773 as $u = [u_1 \dots u_r]$, $v = [v_1 \dots v_c]$ with $u_i \in \mathbb{R}^{m_b}$ and $v_j \in \mathbb{R}^{n_b}$. Then

$$774 \quad \begin{aligned} |u^\top G v| &= \left| \sum_{i=1}^r \sum_{j=1}^c u_i^\top G_{ij} v_j \right| \\ 775 &\leq \sum_{i=1}^r \sum_{j=1}^c |u_i^\top G_{i,j} v_j| \\ 776 &\leq \sum_{i=1}^r \sum_{j=1}^c \|u_i\|_2 \|G_{ij}\|_{\text{op}} \|v_j\|_2 \\ 777 &\leq B(G) \left(\sum_{i=1}^r \|u_i\|_2 \right) \left(\sum_{j=1}^c \|v_j\|_2 \right) \\ 778 &\leq B(G) \sqrt{r} \sqrt{\sum_{i=1}^r \|u_i\|_2^2} \sqrt{c} \sqrt{\sum_{j=1}^c \|v_j\|_2^2} \\ 779 &= \sqrt{rc}B(G), \end{aligned}$$

780 where we used Cauchy–Schwarz applied to the vectors of blockwise ℓ_2 norms. Taking the supremum
 781 over unit u, v gives $\|G\|_{\text{op}} \leq \sqrt{rc}B(G)$.

782 For the dual norm bounds, observe that if norms $\|\cdot\|_a$ and $\|\cdot\|_b$ satisfy $\alpha\|\cdot\|_a \leq \|\cdot\|_b \leq \beta\|\cdot\|_a$,
 783 then their duals satisfy

$$784 \quad \frac{1}{\beta} \|\cdot\|_a^* \leq \|\cdot\|_b^* \leq \frac{1}{\alpha} \|\cdot\|_a^*.$$

785 Applying this with $\|\cdot\|_a = B(\cdot)$, $\|\cdot\|_b = \|\cdot\|_{\text{op}}$, $\alpha = 1$, $\beta = \sqrt{rc}$ yields

$$786 \quad \|G\|_{\text{op},*} \leq B^*(G) \leq \sqrt{rc}\|G\|_{\text{op},*}.$$

787 Finally, for the smoothness bounds, we have for any $X \neq Y$

$$788 \quad \begin{aligned} \frac{\|\nabla f(X) - \nabla f(Y)\|_{\text{op},*}}{\|X - Y\|_{\text{op}}} &\leq \frac{B^*(\nabla f(X) - \nabla f(Y))}{\|X - Y\|_{\text{op}}} \\ 789 &\leq \frac{B^*(\nabla f(X) - \nabla f(Y))}{B(X - Y)} \leq \frac{\sqrt{rc}\|\nabla f(X) - \nabla f(Y)\|_{\text{op},*}}{B(X - Y)} \\ 790 &\leq (rc) \frac{\|\nabla f(X) - \nabla f(Y)\|_{\text{op},*}}{\|X - Y\|_{\text{op}}}. \end{aligned}$$

791 Taking the supremum over X, Y such that $X \neq Y$ immediately yields $L_{\text{op}} \leq L_B \leq (rc)L_{\text{op}}$. \square

810 A.2 CONVERGENCE PROOFS
811812 **Lemma 5** (Descent Lemma). *Suppose that Assumptions 1 and 2 hold for $f : \mathbb{R}^{m \times n} \rightarrow \mathbb{R}$. Then the*
813 *iterations of the algorithm without a regularizer satisfy:*

814
$$f(X_{k+1}) \leq f(X_k) - \eta \|\nabla f(X_k)\| + 2\eta \|\nabla f(X_k) - (1 - \mu)M_k\|_* + \frac{3}{2}L\eta^2.$$

815
816

817 *Proof.* By smoothness,

818
$$\begin{aligned} f(X_{k+1}) &\leq f(X_k) + \langle \nabla f(X_k), X_{k+1} - X_k \rangle + \frac{L}{2} \|X_{k+1} - X_k\|_*^2 \\ &\leq f(X_k) - \eta \langle \nabla f(X_k), \text{Orth}(M_k) \rangle + \frac{L\eta^2}{2} \\ &= f(X_k) - \eta \langle \nabla f(X_k) - (1 - \mu)M_k, \text{Orth}(M_k) \rangle - \eta(1 - \mu) \langle M_k, \text{Orth}(M_k) \rangle + \frac{L\eta^2}{2} \\ &\leq f(X_k) + \eta \|\nabla f(X_k) - (1 - \mu)M_k\|_* \|\text{Orth}(M_k)\| - \eta(1 - \mu) \|M_k\|_* + \frac{L\eta^2}{2} \\ &\leq f(X_k) + \eta \|\nabla f(X_k) - (1 - \mu)M_k\|_* - \eta(1 - \mu) \|M_k\|_* + \frac{L\eta^2}{2} \\ &\leq f(X_k) + 2\eta \|\nabla f(X_k) - (1 - \mu)M_k\|_* - \eta \|\nabla f(X_k)\|_* + \frac{L\eta^2}{2}. \end{aligned}$$

819
820
821
822
823
824
825
826
827
828
829
830

□

831 **Lemma 6.** *Suppose that f satisfies Assumption 1 in some norm $\|\cdot\|$ and is lower bounded by f_* , then*

832
$$\|\nabla f(X)\|_*^2 \leq 2L(f(X) - f_*) .$$

833
834

835 *Proof.* Define

836
$$X_+ = \arg \min_Y \left[f(X) + \langle \nabla f(X), Y - X \rangle + \frac{L}{2} \|Y - X\| \right] = X - \eta \|\nabla f(X)\|_* Z,$$

837
838

839 where Z satisfies $\|Z\| \leq 1$ and $\langle \nabla f(X), Z \rangle = \|\nabla f(X)\|_*$. By smoothness,

840
$$\begin{aligned} f(X_+) &\leq f(X) + \langle \nabla f(X), X_+ - X \rangle + \frac{L}{2} \|X_+ - X\|^2 \\ &= f(X) - \eta \|\nabla f(X)\|_*^2 + \frac{L\eta^2}{2} \|\nabla f(X)\|_*^2 \\ &= f(X) - \eta \left(1 - \frac{L\eta}{2}\right) \|\nabla f(X)\|_*^2. \end{aligned}$$

841
842
843
844
845
846
847
848

849 Plugging $\eta = \frac{1}{L}$ gives

850
$$f_* \leq f(X_+) \leq f(X) - \frac{\|\nabla f(X)\|_*^2}{2L}.$$

851
852

853 Therefore,

854
$$\|\nabla f(X)\|_*^2 \leq 2L(f(X) - f_*) .$$

855
856

□

857 **Lemma 7.** *Let f satisfy Assumptions 1 to 3 in some norm $\|\cdot\|$ with smoothness constant L , stochastic*
858 *gradient variance σ^2 , and ℓ_2 -norm ratio ρ . Let M_τ be defined as*

859
$$M_\tau = \mu M_{\tau-1} + G_\tau,$$

860
861

862
$$X_{\tau+1} = X_\tau - \eta_\tau Z_\tau,$$

863

864 where $\|Z_\tau\| \eta_\tau \leq A$ for all $\tau \leq k$. Then,

865
$$\mathbb{E} [\|\nabla f(X_k) - (1 - \mu)M_k\|_*] \leq \mu^k (1 - \mu)^2 \rho \sigma + \mu^{k+1} \sqrt{2L\Delta_0} + \frac{LA\mu}{1 - \mu} + \rho\sigma \sqrt{\frac{1 - \mu}{1 + \mu}}.$$

866
867

864 *Proof.* Let $M'_k = (1 - \mu)M_k$. We have,

$$\begin{aligned}
 866 \quad \nabla f(X_k) - M'_k &= \nabla f(X_k) - [\mu M'_{k-1} + (1 - \mu)G_k] \\
 867 \quad &= \nabla f(X_k) - \mu M'_{k-1} - (1 - \mu)G_k \\
 868 \quad &= \nabla f(X_k) - G_k - \mu M'_{k-1} + \mu G_k \\
 869 \quad &= \nabla f(X_k) - G_k + \mu \nabla f(X_{k-1}) - \mu M'_{k-1} + \mu G_k - \mu \nabla f(X_{k-1}) \\
 870 \quad &= \nabla f(X_k) - G_k + \mu \nabla f(X_{k-1}) - \mu M'_{k-1} + \mu G_k - \mu \nabla f(X_k) + \mu \nabla f(X_k) - \mu \nabla f(X_{k-1}) \\
 871 \quad &= (1 - \mu)(\nabla f(X_k) - G_k) + \mu(\nabla f(X_{k-1}) - M'_{k-1}) + \mu(\nabla f(X_k) - \nabla f(X_{k-1})). \\
 873
 \end{aligned}$$

874 Let $E_k = \nabla f(X_k) - M'_k$, $S_k = \nabla f(X_k) - G_k$, and $R_k = \nabla f(X_k) - \nabla f(X_{k-1})$. Then the above
875 is,

$$\begin{aligned}
 876 \quad E_k &= \mu E_{k-1} + (1 - \mu)S_k + \mu R_k \\
 877 \quad &= \mu^k E_0 + \sum_{j=0}^{k-1} \mu^j [(1 - \mu)S_{k-j} + \mu R_{k-j}]. \\
 879
 \end{aligned}$$

881 Now observe that

$$882 \quad \|R_{k-j}\|_* = \|\nabla f(X_{k-j}) - \nabla f(X_{k-j-1})\|_* \leq L\|X_k - X_{k-j-1}\| = L\eta_k\|Z_k\| \leq LA.$$

884 Therefore

$$\begin{aligned}
 886 \quad \mathbb{E} [\|E_k\|_*] &\leq \mu^k \mathbb{E} [\|E_0\|_*] + \mathbb{E} \left[\left\| \sum_{j=0}^{k-1} \mu^j [(1 - \mu)S_{k-j} + \mu R_{k-j}] \right\|_* \right] \\
 887 \quad &\leq \mu^k \mathbb{E} [\|E_0\|_*] + \sum_{j=0}^{k-1} \mu^{j+1} \mathbb{E} [\|R_{k-j}\|_*] + \mathbb{E} \left[\left\| \sum_{j=0}^{k-1} \mu^j (1 - \mu)S_{k-j} \right\|_* \right] \\
 888 \quad &\leq \mu^k \mathbb{E} [\|E_0\|_*] + LA \sum_{j=0}^{k-1} \mu^{j+1} + \rho \mathbb{E} \left[\left\| \sum_{j=0}^{k-1} \mu^j (1 - \mu)S_{k-j} \right\|_2 \right] \\
 889 \quad &\leq \mu^k \mathbb{E} [\|E_0\|_*] + \frac{LA\mu}{1 - \mu} + \rho \sqrt{\mathbb{E} \left[\left\| \sum_{j=0}^{k-1} \mu^j (1 - \mu)S_{k-j} \right\|_2^2 \right]} \tag{5}
 \end{aligned}$$

900 We have

$$\begin{aligned}
 902 \quad \mathbb{E} \left[\left\| \sum_{j=0}^{k-1} \mu^j (1 - \mu)S_{k-j} \right\|_2^2 \right] &= \mathbb{E} \left[\sum_{j=0}^{k-1} \sum_{i=0}^{k-1} \mu^j (1 - \mu)^2 \mu^i \langle S_{k-j}, S_{k-i} \rangle \right] \\
 903 \quad &= \sum_{j=0}^{k-1} \mu^{2j} (1 - \mu)^2 \mathbb{E} [\|S_{k-j}\|^2] \\
 904 \quad &\leq \sigma^2 (1 - \mu)^2 \sum_{j=0}^{k-1} \mu^{2j} \\
 905 \quad &\leq \frac{\sigma^2 (1 - \mu)^2}{1 - \mu^2} \\
 906 \quad &= \frac{\sigma^2 (1 - \mu)^2}{(1 - \mu)(1 + \mu)} \\
 907 \quad &= \frac{\sigma^2 (1 - \mu)}{1 + \mu}. \tag{6}
 \end{aligned}$$

918 Using eq. (6) back in eq. (5) we get
 919

$$\mathbb{E} [\|E_k\|_*] \leq \mu^k \mathbb{E} [\|E_0\|_*] + \frac{LA\mu}{1-\mu} + \rho\sigma \sqrt{\frac{1-\mu}{1+\mu}}. \quad (7)$$

920 For the first term,
 921

$$\begin{aligned} \mathbb{E} [\|E_0\|_*] &= \mathbb{E} [\|\nabla f(X_0) - (1-\mu)M_0\|_*] \\ &= \mathbb{E} [\|\nabla f(X_0) - (1-\mu)G_0\|_*] \\ &= \mathbb{E} [\|(1-\mu)(\nabla f(X_0) - G_0) + \mu\nabla f(X_0)\|_*] \\ &\leq (1-\mu)\mathbb{E} [\|\nabla f(X_0) - G_0\|_*] + \mu\|\nabla f(X_0)\|_*. \end{aligned}$$

922 By Lemma 6 we have $\|\nabla f(X_0)\|_* \leq \sqrt{2L(f(X_0) - f_*)}$ and by Assumptions 2 and 3 we have
 923 $\mathbb{E} [\|\nabla f(X_0) - G_0\|_*] \leq \rho\sigma$. Plugging this back in gives
 924

$$\mathbb{E} [\|E_0\|_*] \leq (1-\mu)\rho\sigma + \mu\sqrt{2L\Delta_0},$$

925 where $\Delta_0 = f(X_0) - f_*$. Using the last equation in Equation (7) yields
 926

$$\mathbb{E} [\|E_k\|_*] \leq \mu^k(1-\mu)^2\rho\sigma + \mu^{k+1}\sqrt{2L\Delta_0} + \frac{LA\mu}{1-\mu} + \rho\sigma \sqrt{\frac{1-\mu}{1+\mu}}.$$

927 \square
 928

929 *Proof of Theorem 1.* By Lemmas 5 and 7 we have
 930

$$\begin{aligned} \mathbb{E} [f(X_{k+1})] &\leq \mathbb{E} [f(X_k)] - \eta\mathbb{E} [\|\nabla f(X_k)\|_*] + 2\eta\mathbb{E} [\|\nabla f(X_k) - (1-\mu)M_k\|_*] + \frac{L\eta^2}{2} \\ &\leq \mathbb{E} [f(X_k)] - \eta\mathbb{E} [\|\nabla f(X_k)\|_*] + 2\eta\mu^k(1-\mu)^2\rho\sigma + 2\eta\mu^{k+1}\sqrt{2L\Delta_0} \\ &\quad + \frac{2L\eta^2\mu}{1-\mu} + 2\eta\rho\sigma\sqrt{\frac{1-\mu}{1+\mu}} + \frac{L\eta^2}{2}. \end{aligned}$$

931 Rearranging,
 932

$$\begin{aligned} \mathbb{E} [\|\nabla f(X_k)\|_*] &\leq \frac{1}{\eta} [\mathbb{E} [f(X_k)] - \mathbb{E} [f(X_{k+1})]] + 2\mu^k(1-\mu)^2\rho\sigma + 2\mu^{k+1}\sqrt{2L\Delta_0} \\ &\quad + \frac{L\eta\mu}{1-\mu} + \rho\sigma\sqrt{\frac{1-\mu}{1+\mu}} + \frac{L\eta^2}{2}. \end{aligned}$$

933 Summing up both sides as $k = 0, 1, \dots, T-1$ and telescoping
 934

$$\begin{aligned} \sum_{k=0}^{T-1} \mathbb{E} [\|\nabla f(X_k)\|_*] &\leq \frac{1}{\eta} [f(X_0) - \mathbb{E} [f(X_T)] + 2(1-\mu)^2\rho\sigma \sum_{k=0}^{T-1} \mu^k + 2\mu\sqrt{2L\Delta_0} \sum_{k=0}^{T-1} \mu^k \\ &\quad + \frac{L\eta\mu T}{1-\mu} + \rho\sigma T\sqrt{\frac{1-\mu}{1+\mu}} + \frac{L\eta^2}{2}] \\ &\leq \frac{\Delta_0}{\eta} + 2(1-\mu)\rho\sigma + \frac{2\mu\sqrt{2L\Delta_0}}{1-\mu} + \frac{L\eta\mu T}{1-\mu} + \rho\sigma T\sqrt{\frac{1-\mu}{1+\mu}} + \frac{L\eta^2}{2}. \end{aligned}$$

935 Dividing both sides by T and lower bounding the average on the left hand side by the minimum
 936 yields the theorem's statement. \square
 937

938 *Proof of Theorem 2.* Let Assumption 3 hold for both norms with constants ρ_{op} and ρ_{block} respectively and let $\rho_{\text{BP}} = \frac{\rho_{\text{op}}}{P} + \frac{P-1}{P}\rho_{\text{block}}$. We will later show that ρ_{op} , ρ_{block} , and ρ_{BP} are all bounded by 1. Let $k \leq T-1$. If k is divisible by P , then by Lemma 5 we have
 939

$$\begin{aligned} \mathbb{E} [f(X_{k+1})] &\leq \mathbb{E} [f(X_k)] - \eta_{\text{full}}\mathbb{E} [\|\nabla f(X_k)\|_{\text{op},*}] \\ &\quad + 2\eta_{\text{full}}\mathbb{E} [\|\nabla f(X_k) - (1-\mu)M_k\|_{\text{op},*}] + \frac{L_{\text{op}}\eta_{\text{full}}^2}{2}. \end{aligned} \quad (8)$$

To apply Lemma 7 with the operator norm, we need to ensure that the updates $Z_\tau = \frac{X_\tau - X_{\tau-1}}{\eta_\tau}$ always satisfy $\|Z_\tau\|_{\text{op}}\eta_\tau \leq A$ for all $\tau \leq k$, where η_τ is the stepsize used on the τ -th iteration. Observe that on all τ such that $\tau \% P = 0$, this is trivially true with $A = \eta_{\text{full}}$. On steps where τ is not divisible by P , we have $\|Z_\tau\|_{\text{op}} \leq \sqrt{rc}B(Z_\tau) \leq \sqrt{rc}$ (see Appendix A.1), since on those steps $\eta_\tau = \eta_{\text{block}}$ we therefore have $\|Z_\tau\|_{\text{op}}\eta_\tau \leq \eta_{\text{block}}\sqrt{rc}$. Therefore in all cases, $\|Z_\tau\|_{\text{op}}\eta_\tau \leq \max(\eta_{\text{block}}\sqrt{rc}, \eta_{\text{full}})$ and we can apply Lemma 7 to get

$$\begin{aligned} \mathbb{E} [\|\nabla f(X_k) - (1 - \mu)M_k\|_{\text{op},*}] &\leq \mu^k(1 - \mu)^2\rho_{\text{op}}\sigma + \mu^{k+1}\sqrt{2L_{\text{op}}\Delta_0} \\ &\quad + \frac{L_{\text{op}}\mu}{1 - \mu} \max(\eta_{\text{full}}, \eta_{\text{block}}\sqrt{rc}) + \rho_{\text{op}}\sigma\sqrt{\frac{1 - \mu}{1 + \mu}}. \end{aligned}$$

We can then use this to bound the third term on the right hand side of Equation (8) to get

$$\begin{aligned} \mathbb{E} [f(X_{k+1})] &\leq \mathbb{E} [f(X_k)] - \eta_{\text{full}}\mathbb{E} [\|\nabla f(X_k)\|_{\text{op},*}] + 2\eta_{\text{full}}\mu^k(1 - \mu)^2\rho_{\text{op}}\sigma \\ &\quad + 2\eta_{\text{full}}\mu^{k+1}\sqrt{2L_{\text{op}}\Delta_0} + \frac{2L_{\text{op}}\eta^2\sqrt{rc}\mu}{1 - \mu} + 2\eta\rho_{\text{op}}\sigma\sqrt{\frac{1 - \mu}{1 + \mu}} + \frac{L_{\text{op}}\eta^2}{2}. \end{aligned} \quad (9)$$

Alternatively, if k is not divisible by P , then similar to the above we first use Lemma 5 and the fact that $B^*(\nabla f(X_k)) \geq \|\nabla f(X_k)\|_{\text{op},*}$ to get

$$\begin{aligned} \mathbb{E} [f(X_{k+1})] &\leq \mathbb{E} [f(X_k)] - \eta_{\text{block}}\mathbb{E} [\|\nabla f(X_k)\|_{\text{op},*}] + 2\eta_{\text{block}}\mathbb{E} [B^*(\nabla f(X_k) - (1 - \mu)M_k)] \\ &\quad + \frac{L_B\eta_{\text{block}}^2}{2}. \end{aligned} \quad (10)$$

We now apply Lemma 7 to the block norm. Note that if τ is not divisible by P , $B(Z_\tau)\eta_\tau = B(Z_\tau)\eta_{\text{block}} \leq \eta_{\text{block}}$. If τ is divisible by P , then $B(Z_\tau)\eta_\tau = B(Z_\tau)\eta_{\text{full}} \leq \|Z_\tau\|_{\text{op}}\eta_{\text{full}} \leq \eta_{\text{full}}$. Therefore by Lemma 7 we have

$$\begin{aligned} \mathbb{E} [B^*(\nabla f(X_k) - (1 - \mu)M_k)] &\leq \mu^k(1 - \mu)^2\rho_{\text{block}}\sigma + \mu^{k+1}\sqrt{2L_B\Delta_0} + \frac{L_B \max(\eta_{\text{block}}, \eta_{\text{full}})\mu}{1 - \mu} \\ &\quad + \rho_{\text{block}}\sigma\sqrt{\frac{1 - \mu}{1 + \mu}}. \end{aligned} \quad (11)$$

Using Equation (11) in Equation (10) we obtain

$$\begin{aligned} \mathbb{E} [f(X_{k+1})] &\leq \mathbb{E} [f(X_k)] - \eta_{\text{block}}\mathbb{E} [\|\nabla f(X_k)\|_{\text{op},*}] + \frac{L_B\eta_{\text{block}}^2}{2} \\ &\quad + 2\eta_{\text{block}} \left[\mu^k(1 - \mu)^2\rho_{\text{block}}\sigma + \mu^{k+1}\sqrt{2L_B\Delta_0} + \frac{L_B \max(\eta_{\text{block}}, \eta_{\text{full}})\mu}{1 - \mu} + \rho_{\text{block}}\sigma\sqrt{\frac{1 - \mu}{1 + \mu}} \right]. \end{aligned} \quad (12)$$

Let $S_P = \{k < T \mid k \pmod P = 0\}$ and $S_B = \{k < T \mid k \pmod P \neq 0\}$. By rearranging the one-step descent inequalities and using Equations (9) and (12) we sum over $k = 0, \dots, T-1$:

$$\begin{aligned} \sum_{k=0}^{T-1} (1_{k \in S_P}\eta_{\text{full}} + 1_{k \in S_B}\eta_{\text{block}})\mathbb{E} [\|\nabla f(X_k)\|_{\text{op},*}] &\leq \sum_{k=0}^{T-1} (\mathbb{E} [f(X_k)] - \mathbb{E} [f(X_{k+1})]) \\ &\quad + \sum_{k \in S_P} (\text{Error}_k^{\text{full}}) + \sum_{k \in S_B} (\text{Error}_k^{\text{block}}), \end{aligned} \quad (13)$$

where

$$\begin{aligned} \text{Error}_k^{\text{full}} &= 2\eta_{\text{full}}\mu^k(1 - \mu)^2\rho_{\text{op}}\sigma + 2\eta_{\text{full}}\mu^{k+1}\sqrt{2L_{\text{op}}\Delta_0} + \frac{2L_{\text{op}}\eta_{\text{full}} \max(\eta_{\text{block}}\sqrt{rc}, \eta_{\text{full}})\mu}{1 - \mu} \\ &\quad + 2\eta_{\text{full}}\rho_{\text{op}}\sigma\sqrt{\frac{1 - \mu}{1 + \mu}} + \frac{L_{\text{op}}\eta_{\text{full}}^2}{2}, \end{aligned}$$

$$\begin{aligned} \text{Error}_k^{\text{block}} &= 2\eta_{\text{block}}\mu^k(1 - \mu)^2\rho_{\text{block}}\sigma + 2\eta_{\text{block}}\mu^{k+1}\sqrt{2L_B\Delta_0} + \frac{2L_B\eta_{\text{block}} \max(\eta_{\text{block}}, \eta_{\text{full}})\mu}{1 - \mu} \\ &\quad + 2\eta_{\text{block}}\rho_{\text{block}}\sigma\sqrt{\frac{1 - \mu}{1 + \mu}} + \frac{L_B\eta_{\text{block}}^2}{2}. \end{aligned}$$

1026 The first term on the right hand side of eq. (13) is a telescoping sum bounded by $\Delta_0 = f(X_0) - f_*$.
 1027 For the error terms dependent on μ^k , we can form a simple upper bound by summing over all k and
 1028 using the larger constants (L_B, ρ_{block}):

1029 Momentum-dependent error

$$\begin{aligned}
 1031 &= \sum_{k \in S_P} \left[2\eta_{\text{full}}\mu^k(1-\mu)^2\rho_{\text{op}}\sigma + 2\eta_{\text{full}}\mu^{k+1}\sqrt{2L_{\text{op}}\Delta_0} \right] \\
 1032 &\quad + \sum_{k \in S_B} \left[2\eta_{\text{block}}\mu^k(1-\mu)^2\rho_{\text{block}}\sigma + 2\eta_{\text{block}}\mu^{k+1}\sqrt{2L_B\Delta_0} \right] \\
 1033 &\leq 4 \sum_{k=0}^{T-1} \left(\mu^k(1-\mu)^2 \max(\eta_{\text{full}}\rho_{\text{op}}, \eta_{\text{block}}\rho_{\text{block}})\sigma + \mu^{k+1} \max(\eta_{\text{full}}\sqrt{L_{\text{op}}}, \eta_{\text{block}}\sqrt{L_B})\sqrt{2L_B\Delta_0} \right) \\
 1034 &\leq 4 \left((1-\mu) \max(\eta_{\text{full}}\rho_{\text{op}}, \eta_{\text{block}}\rho_{\text{block}})\sigma + \frac{\mu \max(\eta_{\text{full}}\sqrt{L_{\text{op}}}, \eta_{\text{block}}\sqrt{L_B})\sqrt{2\Delta_0}}{1-\mu} \right).
 \end{aligned}$$

1041 For the other terms, we sum them proportionally. Observe that $|S_P| = T/P$ and $|S_B| = T(P-1)/P$, as we assume that T is divisible by P . Therefore,

$$\begin{aligned}
 1044 \text{Constant error} &= \sum_{k \in S_P} \left(\frac{L_{\text{op}}\eta_{\text{full}}^2}{2} + \frac{2L_{\text{op}}\max(\eta_{\text{full}}\eta_{\text{block}}\sqrt{rc}, \eta_{\text{full}}^2)\mu}{1-\mu} + 2\eta_{\text{full}}\rho_{\text{op}}\sigma\sqrt{\frac{1-\mu}{1+\mu}} \right) \\
 1045 &\quad + \sum_{k \in S_B} \left(\frac{L_B\eta_{\text{block}}^2}{2} + \frac{2L_B\max(\eta_{\text{full}}\eta_{\text{block}}, \eta_{\text{block}}^2)\mu}{1-\mu} + 2\eta_{\text{block}}\rho_{\text{block}}\sigma\sqrt{\frac{1-\mu}{1+\mu}} \right) \\
 1046 &= T \left(\frac{\eta_{\text{full}}^2 L_{\text{op}}}{2P} + \frac{L_B\eta_{\text{block}}^2(P-1)}{2P} + \right. \\
 1047 &\quad + \frac{2\mu}{1-\mu} \left[\frac{L_{\text{op}}\max(\eta_{\text{full}}\eta_{\text{block}}\sqrt{rc}, \eta_{\text{full}}^2)}{P} + \frac{L_B\max(\eta_{\text{full}}\eta_{\text{block}}, \eta_{\text{block}}^2)(P-1)}{P} \right] \\
 1048 &\quad \left. + 2\sigma\sqrt{\frac{1-\mu}{1+\mu}} \left[\frac{\eta_{\text{full}}\rho_{\text{op}}}{P} + \frac{\eta_{\text{block}}\rho_{\text{block}}(P-1)}{P} \right] \right)
 \end{aligned}$$

1049 Observe that,

$$\begin{aligned}
 1050 &\sum_{k=0}^{T-1} (1_{k \in S_P}\eta_{\text{full}} + 1_{k \in S_B}\eta_{\text{block}})\mathbb{E}[\|\nabla f(X_k)\|_{\text{op},*}] \geq T \left[\frac{\eta_{\text{full}}}{P} + \frac{\eta_{\text{block}}(P-1)}{P} \right] \min_k \mathbb{E}[\|\nabla f(X_k)\|_{\text{op},*}] \\
 1051 &= T\bar{\eta} \min_k \mathbb{E}[\|\nabla f(X_k)\|_{\text{op},*}].
 \end{aligned}$$

1052 Observe that for the operator norm and the block spectrum norm, we have $\rho_{\text{op}} \leq 1$ and $\rho_{\text{block}} \leq 1$
 1053 by Lemma 3. Using this and combining all the error parts we get

$$\begin{aligned}
 1054 &\bar{\eta}T \min_k \mathbb{E}[\|\nabla f(X_k)\|_{\text{op},*}] \leq \Delta_0 + 4(1-\mu)\sigma\eta_{\text{max}} + \frac{6\mu\sqrt{\Delta_0}}{1-\mu} \max(\eta_{\text{full}}\sqrt{L_{\text{op}}}, \eta_{\text{block}}\sqrt{L_B}) \\
 1055 &\quad + T \left(\frac{\eta_{\text{full}}^2 L_{\text{op}}}{2P} + \frac{L_B\eta_{\text{block}}^2(P-1)}{2P} + 2\sigma\sqrt{\frac{1-\mu}{1+\mu}}\bar{\eta} \right. \\
 1056 &\quad \left. + \frac{2\mu}{1-\mu} \left[\frac{L_{\text{op}}\eta_{\text{full}}\max(\eta_{\text{block}}\sqrt{rc}, \eta_{\text{full}})}{P} + \frac{L_B\eta_{\text{block}}\max(\eta_{\text{full}}, \eta_{\text{block}})(P-1)}{P} \right] \right).
 \end{aligned}$$

1057 Dividing both sides by $\bar{\eta}T$ yields

$$\begin{aligned}
 1058 &\min_{k < T} \mathbb{E}[\|\nabla f(X_k)\|_{\text{op},*}] \leq \frac{\Delta_0}{\bar{\eta}T} + \frac{4(1-\mu)\sigma\eta_{\text{max}}}{\bar{\eta}T} + \frac{6\mu\sqrt{\Delta_0}}{1-\mu} \cdot \frac{\max\{\eta_{\text{full}}\sqrt{L_{\text{op}}}, \eta_{\text{block}}\sqrt{L_B}\}}{\bar{\eta}T} \\
 1059 &\quad + \frac{1}{\bar{\eta}} \left[\frac{L_{\text{op}}\eta_{\text{full}}^2}{2P} + \frac{L_B\eta_{\text{block}}^2(P-1)}{2P} \right. \\
 1060 &\quad \left. + \frac{2\mu}{1-\mu} \left(\frac{L_{\text{op}}\eta_{\text{full}}\max(\eta_{\text{block}}\sqrt{rc}, \eta_{\text{full}})}{P} + \frac{L_B\eta_{\text{block}}\max(\eta_{\text{full}}, \eta_{\text{block}})(P-1)}{P} \right) \right] + 2\sigma\sqrt{\frac{1-\mu}{1+\mu}},
 \end{aligned}$$

1080 where

1081
1082
$$\bar{\eta} = \frac{\eta_{\text{full}}}{P} + \frac{P-1}{P} \eta_{\text{block}}, \quad \eta_{\text{max}} = \max\{\eta_{\text{full}}, \eta_{\text{block}}\}.$$

1083
1084 \square
1085

1086 **B ADDITIONAL ALGORITHMS, RESULTS, AND EXPERIMENTAL DETAILS**
10871088 The orthogonalization via Newton Schulz iterations procedure is stated as Algorithm 2.
10891090 **Algorithm 2:** Orthogonalize-via-NS($G, K, \varepsilon = 10^{-7}$)
10911092 1 $a \leftarrow 2, b \leftarrow -1.5, c \leftarrow 0.5;$
1093 2 $X \leftarrow G/(\|G\| + \varepsilon);$
1094 3 **for** $t \leftarrow 1$ **to** K **do**
1095 4 $A \leftarrow XX^\top;$
1096 5 $B \leftarrow bA + cA^2;$
1097 6 $X \leftarrow aX + BX;$
1098 7 **return** $X;$
10991100 All the architectural hyperparameters and learning rates used are given in Table 4 below. We used
1101 the learning rates from (Liu et al., 2025) as a starting point for each run. We found at a smaller scale
1102 that the learning rates recommended therein could be increased by a factor of ≈ 3 with no harm to
1103 convergence for the baseline (Muon) algorithm, and we scaled the other learning rates accordingly.
1104 Nevertheless, we do two experiments with smaller learning rates. We use GQA (Ainslie et al.,
1105 2023), RoPE (Su et al., 2024), bf16 mixed-precision training, and a weight decay value of 0.1. We
1106 also apply gradient clipping with value 1.0 to the parameters optimized by AdamW (mainly 1D
1107 parameters and the input embedding). We use cosine decay with no warmup for the 960M and 1.2B
1108 experiments and the Warmup-Stable-Decay (WSD) schedule (Hägele et al., 2024) with linear decay
1109 to 4.2×10^{-5} for the 8B model.
11101111 Table 4: Section 4.2 experiments hyperparameters (sequence length = 8K, Batch size=128 sequences
1112 for 960M/1.2B models and 256 sequences for 8B models).

Model	Layers	Heads	Query Groups	Hidden Size	(DP, TP)	LR ($\times 10^{-3}$)	Tokens (B)
960M	12	16	4	1536	(2, 4)	3.503	9.503
1.2B	14	16	4	1792	(2, 4)	3.291	14.143
1.2B (3x long, larger lr)	14	16	4	1792	(2, 4)	3.291	42.143
1.2B (3x long, smaller lr)	14	16	4	1792	(2, 4)	0.86	42.143
8B (smaller lr)	32	32	8	4096	(4, 8)	0.6	9.99
8B (larger lr)	32	32	8	4096	(4, 8)	1.2	9.99

1113
1114 We report the training curves for the 960M model in Figure 4, for the 1.2B model in Figure 5, for
1115 the 1.2B model trained to 3x Chinchilla with smaller learning rate in Figure 7, with larger learning
1116 in Figure 6, and for the 8B model in Figure 10 (smaller learning rate) and Figure 9 (larger learning
1117 rate). Our main observation here is that even after doing RMS norm adjustment (i.e. update is scaled
1118 by $\sqrt{\max(A, B)}$ where A and B are the dimensions of the update matrix, which scale inversely with
1119 blocking), BlockMuon can become unstable with larger learning rates. On the contrary, MuonBP
1120 does not.1121 A reason why this might be the case is that BlockMuon almost always causes the parameter norms
1122 to grow larger over time compared to Muon or MuonBP, as can be seen in Table 5. This holds even
1123 when we use small learning rates and learning rate adjustment.
11241125
1126
1127
1128
1129
1130
1131
1132
1133

1134

1135

1136

1137

1138

1139

1140

1141

1142

1143

1144

1145

1146

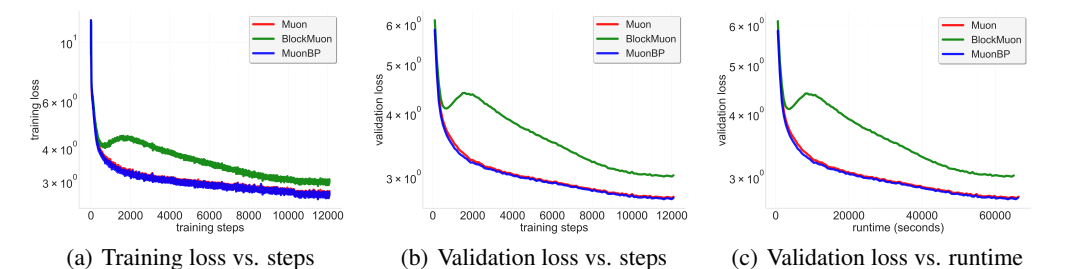


Figure 4: 960M model. Comparison of baseline, block, and periodic orthogonal block methods across training steps and wall-clock time.

1147

1148

1149

1150

1151

1152

1153

1154

1155

1156

1157

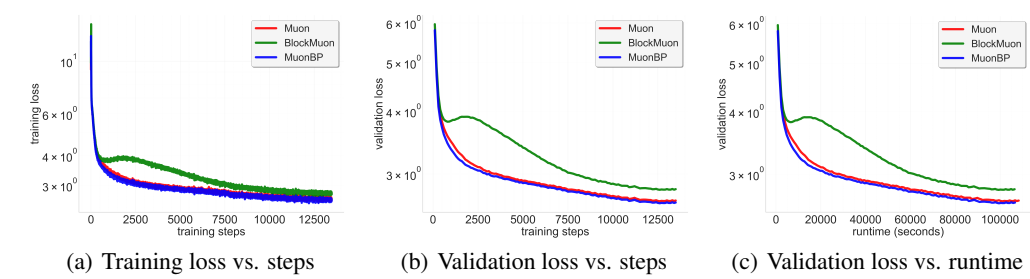


Figure 5: 1.2B model. Comparison of baseline, block, and periodic orthogonal block methods across training steps and wall-clock time.

1158

1159

1160

1161

1162

1163

1164

1165

1166

1167

1168

1169

1170

1171

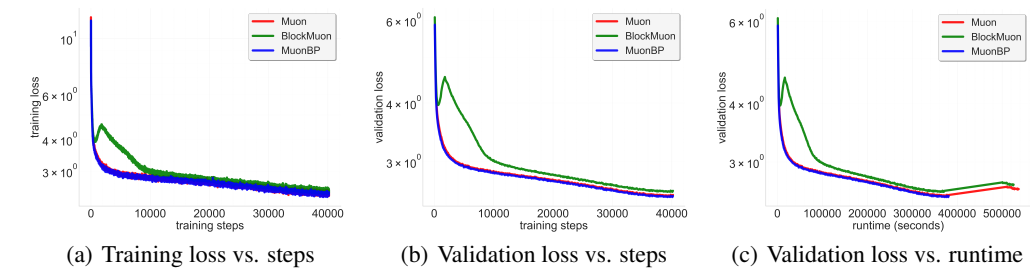


Figure 6: 1.2B model (larger lr), trained to 3x Chinchilla. Comparison of baseline, block, and periodic orthogonal block methods across training steps and wall-clock time.

1172

1173

1174

1175

1176

1177

1178

1179

1180

1181

1182

1183

1184

1185

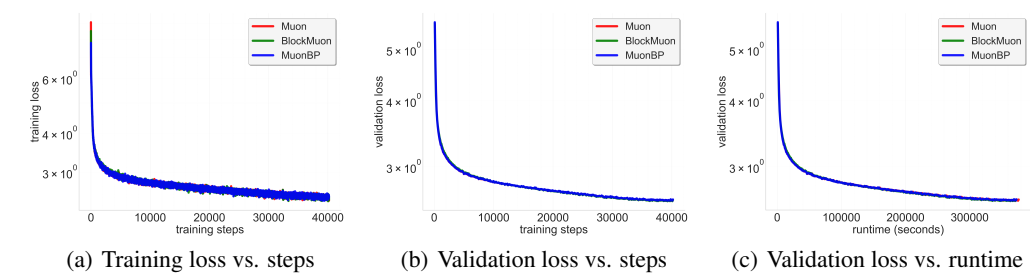
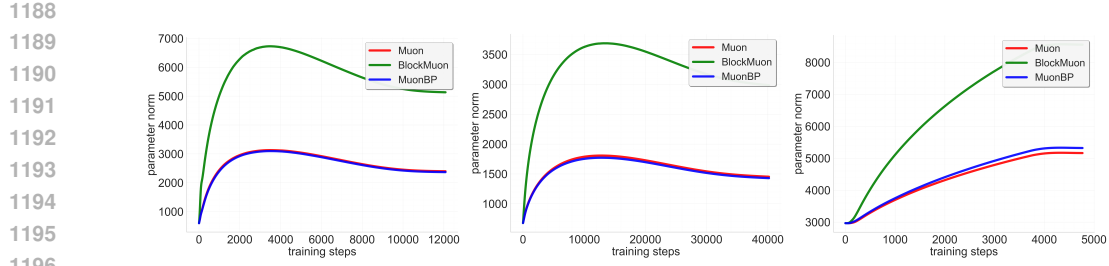


Figure 7: 1.2B model (smaller lr), trained to 3x Chinchilla. Comparison of baseline, block, and periodic orthogonal block methods across training steps and wall-clock time.



1197
1198
1199
1200
1201
1202
1203
1204
1205
1206
1207
1208
1209
1210
1211
1212
1213
1214
1215
1216
1217
1218
1219
1220
1221
1222
1223
1224
1225
1226
1227
1228
1229
1230
1231
1232
1233
1234
1235
1236
1237
1238
1239
1240
1241

Figure 8: Comparison of parameter norms using Muon, BlockMuon, and MuonBP over training on 960M model (left), 1.2B model 3x-Chinchilla with smaller lr (center), and 8B model (right).

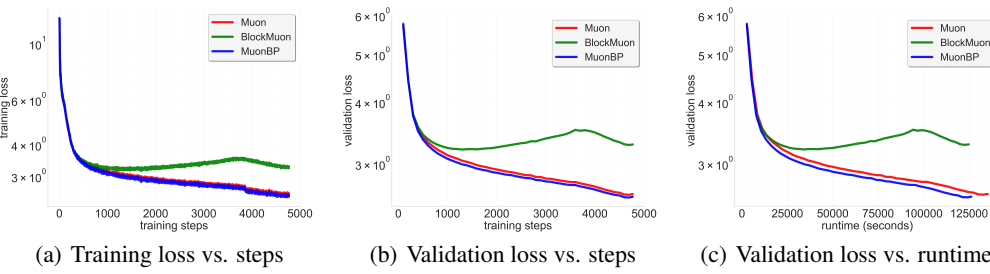


Figure 9: 8B model (larger lr). Comparison of baseline, block, and periodic orthogonal block methods across training steps and wall-clock time.

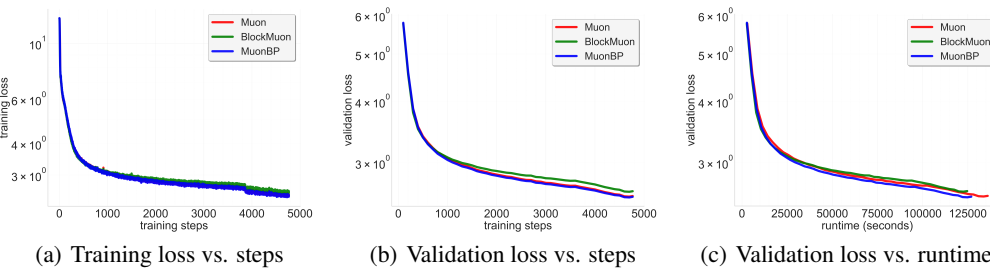


Figure 10: 8B model (smaller lr). Comparison of baseline, block, and periodic orthogonal block methods across training steps and wall-clock time.

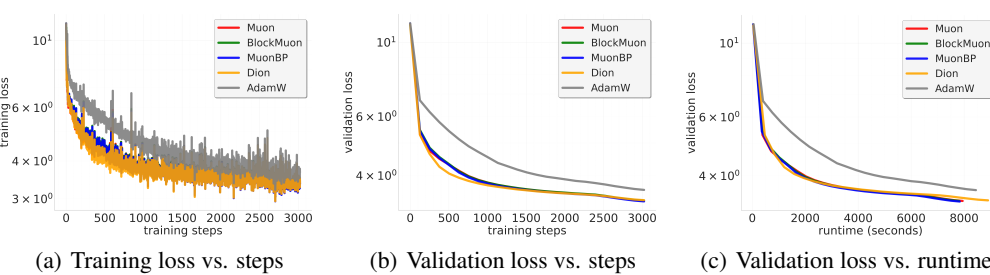


Figure 11: 160M model training with 2-way FSDP2 and 4-way TP. Comparison of Baseline, Block-Muon, MuonBP, and Dion across training steps and wall-clock time.

1242
 1243
 1244
 1245
 1246
 1247
 1248
 1249
 1250
 1251
 1252
 1253
 1254
 1255
 1256
 1257

1258 Table 5: Validation/Training perplexity (*lower is better*) and average parameter norm. Best perplexities
 1259 within each model size are in **bold**.

Model	Method	Val PPL	Train PPL	Param Norm
960M	Muon	15.33	13.44	2680
	BlockMuon	20.29	18.08	5702
	MuonBP	15.12	13.21	2648
1.2B	Muon	14.13	12.83	4237
	BlockMuon	16.28	14.86	7225
	MuonBP	13.78	12.44	4195
1.2B (3 \times , large lr)	Muon	12.62	10.88	2681
	BlockMuon	13.29	11.51	5521
	MuonBP	12.45	10.71	2868
1.2B (3 \times , small lr)	Muon	13.26	11.40	1602
	BlockMuon	13.22	11.29	3242
	MuonBP	13.30	11.39	1571
8B	Muon	12.90	11.74	4369
	BlockMuon	13.68	12.62	6680
	MuonBP	12.77	11.59	4471
8B (large lr)	Muon	13.40	12.39	6841
	BlockMuon	24.68	23.17	11 496
	MuonBP	12.97	11.93	7063

1281
 1282
 1283
 1284
 1285
 1286
 1287
 1288
 1289
 1290
 1291
 1292
 1293
 1294
 1295